nature ecology & evolution

Article

https://doi.org/10.1038/s41559-022-01970-1

A surge in obsidian exploitation more than 1.2 million years ago at Simbiro III (Melka Kunture, Upper Awash, Ethiopia)

In the format provided by the authors and unedited

Contents:

Supplementary Information A. History of Studies

The Monumental Section of the Simbiro gully was discovered in the 1960s but was directly investigated in the final days of 1973, when a large *Pelorovis oldowayensis* skull, still partially embedded, came to light due to heavy rains and erosion (**Supplementary Information Fig. A1-2**). After a brief rescue operation (**Supplementary Information Fig. A3**), the fossil was preserved and is currently kept at the National Museum in Addis Ababa. Proper excavations were conducted during three brief field seasons at the end of 1974, 1975, and 1976 (**Supplementary Information Fig. A4-5**). Levels C and D were excavated in 1974 and 1975. It was often difficult to discriminate between them. The last field season was focused on levels A and B. Pictures, plans, notes, and manuscripts were prepared by Jean Chavaillon and his team. Notably, from 1974 to 1976, Ouardya Oussedik directed the field research and took daily notes on the ongoing operations. A report on the 1974 excavations was published [1,] and another one was prepared in 1976 but not published.

The pictures, plans, notes, and manuscripts are kept in the archives of the archeological mission. Oussedik's notes, hastily handwritten on the spot in French, generally refer to daily activities and tasks. However, she added sketches and details which are useful to better understand how level C deposited: bivalves are noticed (28-XI-74 and 27-XI-75); smaller artifacts are found within a sandy deposit, larger ones within gravels (27-XI-75); the artifacts are often in heaps and the preservation of the surfaces is uneven (28-XI-75); there are "clouds" ("*nébuleuses*") of artifacts (1- XII-75) – assumedly small ones; the color of artifacts varies from greyish (bad preservation) to black (good preservation) (2-XII-75); most artifacts were in a vertical position, and large artifacts are found more frequently deeper into the deposit, with the smaller ones above them (9-XII-75).

Then, in 2004, when Marcello Piperno was the director of the Italian Archaeological Mission, another small test was dug in level C, 8 m south of Oussedik's trench in that level (**Supplementary Information Fig. A5**). Overall, approximately 18.7 m^2 of the MS has been excavated in the last 50 years, with 4 main archeological levels: from top to bottom, levels A, B, C, D (**Supplementary Information Table A1 and Supplementary Information Fig. A5**). In the following years the site was quoted in general terms in the literature but never published in detail. Samples were later taken for various purposes, notably for a PhD thesis on palaeomagnetism defended by P. Cressier in 1980 [2]. More recently, the obsidian composition was analyzed by F.X. Le Bourdonnec in the framework of his PhD thesis defended in 2007 [3], while L. Morgan took a sample providing the first $^{40}Ar/^{39}Ar$ dates [4]. To date, the site has not attracted much attention [1,5].

Since 2017, fieldwork has been resumed in the Simbiro gully by the now Italo-Spanish Archaeological Mission, directed by Margherita Mussi, allowing a full reassessment. A fifth level, level E, not discussed here, is currently under excavations at the bottom of the creek.

Supplementary Information Table A1. The excavated surface of the archeological levels of the MS (Chavaillon's and Piperno's fieldwork).

Level	Area (m^2)
Level A	4.4
Level B	6.6
Level C	4.1
Level C (Piperno`s excavations)	0.7
Level D	2.9
Total surface	**18.7**

Supplementary Information Fig. A1. The MS of Simbiro III in 1974 (archives of the Italo-Spanish Archaeological Mission at Melka Kunture).

Supplementary Information Fig. A2. The *Pelorovis oldowayensis* skull still partially embedded in the MS just below level B at the time of discovery in 1973 (archives of the Italo-Spanish Archaeological Mission at Melka Kunture).

Supplementary Information Fig. B3. The *Pelorovis oldowayensis* skull under excavation in 1973 (archives of the Italo-Spanish Archaeological Mission at Melka Kunture).

Supplementary Information Fig. A4. Fieldwork at the MS in 1975: levels B (right) and A (left) (archives of the Italo-Spanish Archaeological Mission at Melka Kunture).

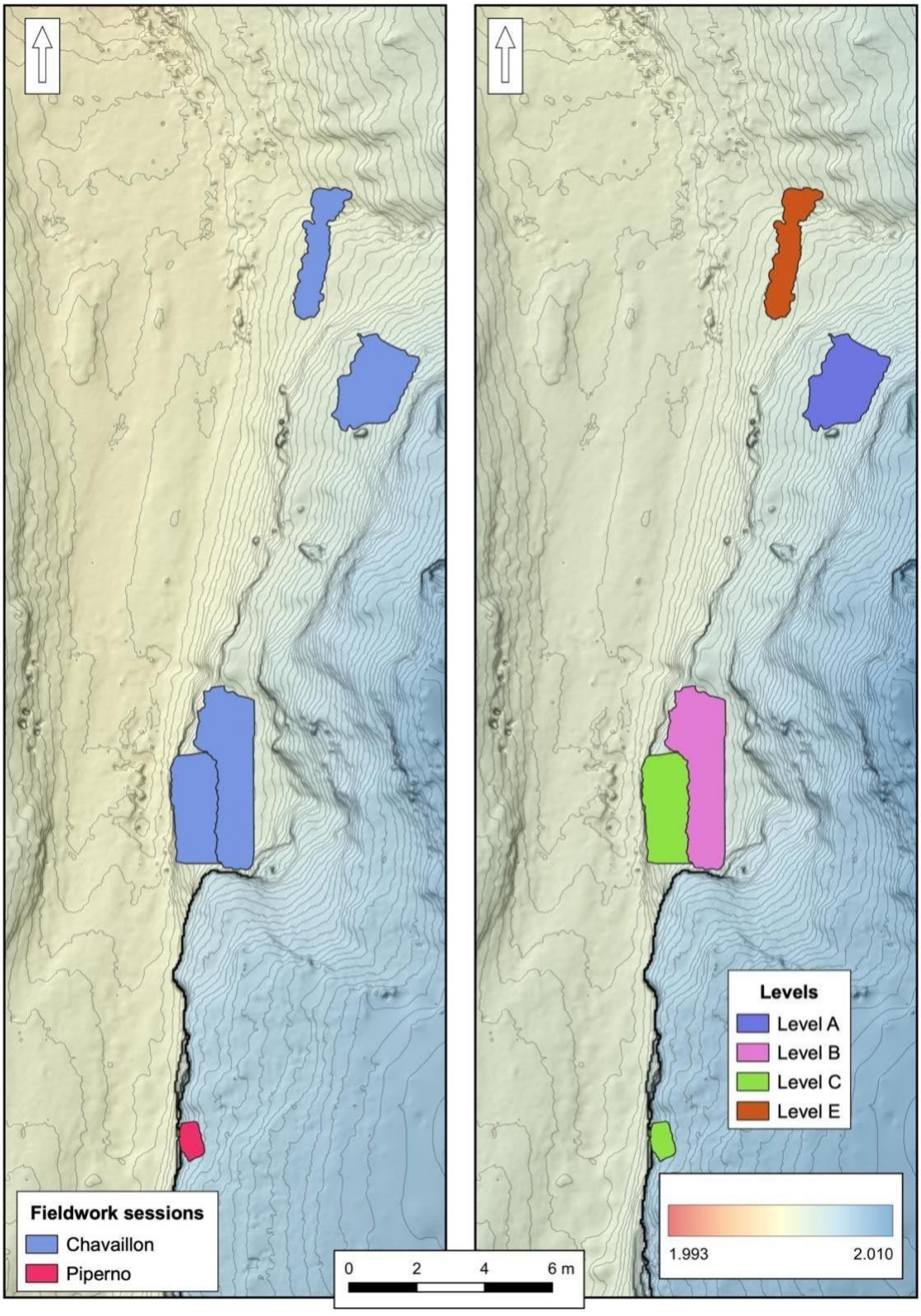

Supplementary Information Fig. A5. Excavated surfaces and levels of the MS (Chavaillon's and Piperno's fieldwork).

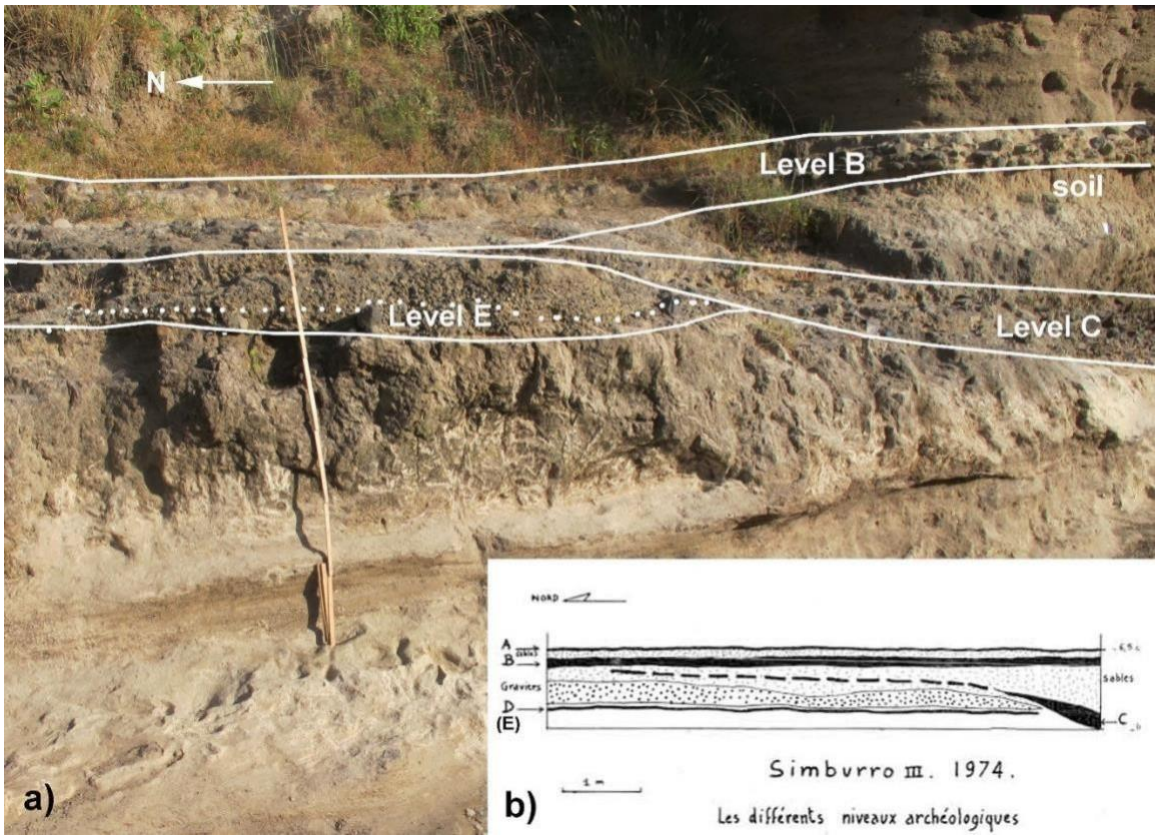

Supplementary Information Fig. A6. a) detail of the extant northern part of the MS, with archaeological levels B, C, E. Note that most of Level B was removed in 1974-1976, as better seen in **Supplementary Information Fig. A4**. Level D is not recorded in this part of the sequence; b) the schematic stratigraphic sequence published by Oussedik[1]. Note that the archaeological level D recorded here is now understood to be instead level E.

Supplementary Information B. Paleoenvironmental data

Supplementary Information B1. The faunal remains

The collection of large mammals from the MS has been briefly described [6]. It has approximately 80 specimens identified at least to family level. Only a few are from level C, and most are from levels A, B, and E. Even if not strictly contemporaneous, they do provide valuable indications about the age and environment of the site. In contrast to other sites at Melka Kunture, there is virtually no unidentifiable fragment. More than half of the identifiable specimens belong to the Bovidae. Approximately two- thirds of those that can be identified to the family level are alcelaphins, a proportion more similar to that of the late Early Pleistocene site of Gombore II dated approximately 1 Ma [7] than to earlier sites, where the dominance of alcelaphins is overwhelming. They include at least three taxa (**Supplementary Information Table B1**). *Megalotragus* can be recognized thanks to its large size (**Supplementary Information Fig. B1**), while an identified *Connochaetes* (**SI Supplementary Information Fig. B2**) is certainly closer to *C. gentryi leptoceras* from Garba IVD, also at Melka Kunture, and dated 1.95 Ma [7], than to the modern *C. taurinus*, the blue wildebeest. There may be two species of *Damaliscus*, the modern tsessebe *D. lunatus* and perhaps the larger, extinct *D. niro*, but *Hippotragus* would be an alternative identification, especially as some teeth are hippotragin ones. Several specimens belong to the Bovini, and the MS is noticeable in documenting, as in the KBS and Okote members of Koobi Fora, the co-occurrence of two species of *Pelorovis*, *P. oldowayensis*, and *P. turkanensis* (**SI Supplementary Information Fig. B3**), although uncertainty about the precise stratigraphic origin of the former leaves some doubts about their exact contemporaneity. Other faunal elements are *Equus* [6]. There is no definite evidence of hipparions, even though they are present at later sites of Melka Kunture. A suid larger than *Phacochoerus* was further identified. Simbiro also yielded the most complete specimen of the cercopithecid *Theropithecus* so far discovered at Melka Kunture, which was collected just north of the MS below archeological level E. It was identified as *T*. cf. *oswaldi* by Beaudet et al. [8] (**SI Supplementary Information Fig. B4**), but the short, deep muzzle shows that it can be definitely identified as *T. oswaldi*.

Supplementary Information Table B1. Faunal remains from the MS excavations.

Taxon		***n.***
Bovidae	***Alcelaphini***	
	Damaliscus cf. *lunatus*	3
	Connochaetes cf. *gentryi*	5
	Megalotragus sp.	5
	Other Alcelaphini	5
	Bovini	
	Pelorovis turkanensis	1
	Pelorovis oldowayensis	1
	Other Bovini	11
	Hippotragini	
	Hippotragus? sp.	3
	Reduncini	1
	Unidentified *Bovidae*	12
Equidae (probably all *Equus* sp.)		13
Hippopotamus cf. *amphibius*		24
Suidae (not *Phacochoerus*)		1
Theropithecus oswaldi		1

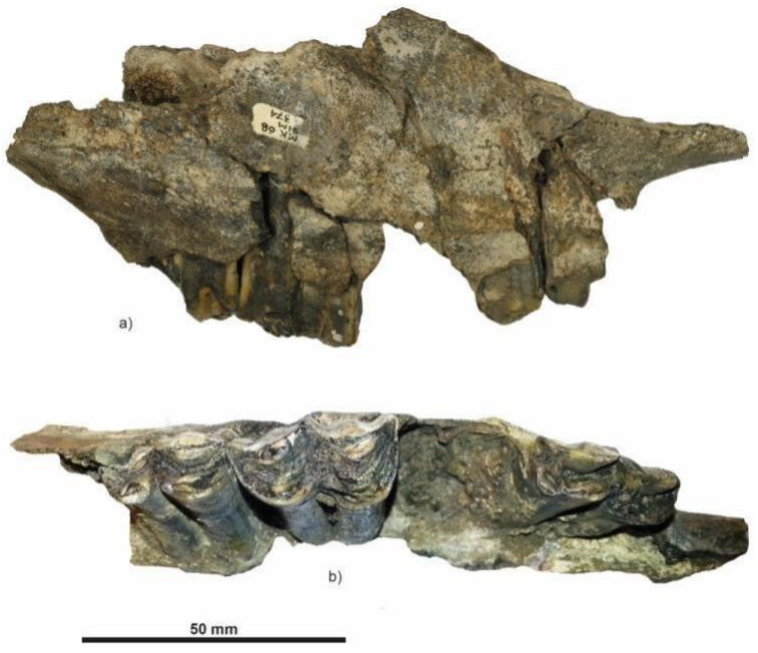

Supplementary Information Fig. B1. Specimen Sim III-374: maxilla of *Megalotragus* sp., in lateral and occlusal view.

Supplementary Information Fig. B2. Specimen SIM III-197: left horncore of *Connochaetes gentryi* in posterior (a) and antero-dorsal (b) view.

Supplementary Information Fig. B3. Specimen SIM III-537: right horn of *P. turkanensis* in posterior (a) and dorsal (b) view.

Supplementary Information Fig. B4. *Theropithecus oswaldi* maxilla from level E in 3D.

Supplementary Information B2. Phytoliths

Nine samples for phytolith analysis were taken from various levels of the MS, including archeological levels B, C, and D (**Supplementary Information Fig. B5**). 3-5 g of dry sediment was processed following standard protocols including the removal of carbonates with HCl, oxidation of organic matter with H_2O_2, removal of clays by decantation, and densimetric separation of minerals and biogenic silica particles using $ZnBr_2$ heavy liquid set at density 2.3 g/cm^3. Phytoliths, diatoms (entire valves distinguished according to their overall shape round or pennate), sponges (distinguished as spicules with preserved tip, asteroscleres, and birotulate gemmuloscleres), and stomatocysts of Chrysophyceae were counted separately, but taxonomical identification was only carried out for phytoliths. Absolute phytolith counts range from 142 to 702 morphotypes including diagnostic and non-diagnostic morphotypes or morphotypes for which taxonomical identification is not yet established (**Supplementary Information Table B2**). More than 67 different phytolith morphotypes were identified; those observed only once, and unknown, were lumped into a single category after counting. Absolute counts of grass silica short cell phytoliths (GSSCs) are >130 (270 in average), except for sample 3 (sum GSSC=24). Percentages were calculated on the total sum of particles for diatoms, sponges and cysts, and on the total sum of phytoliths for phytolith morphotypes.

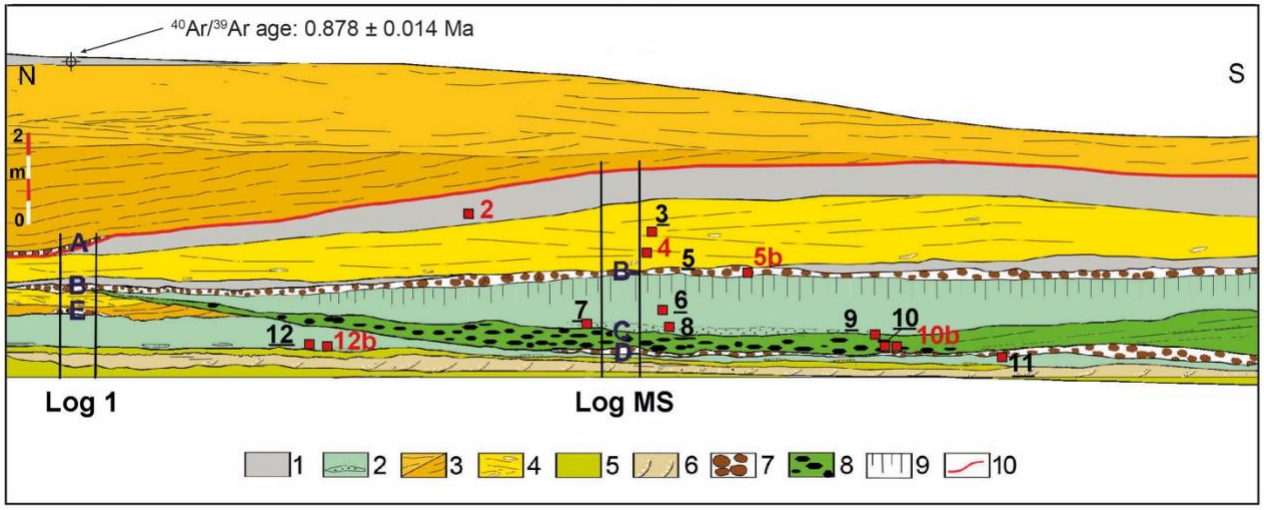

Supplementary Information Fig. B5. The analyzed phytolith samples placed on the stratigraphic sequence with productive samples identified by black numbers. For the sedimentary interpretation cfr. the **Extended Data 2** legend.

Supplementary Information Table B2. Categories of phytoliths and other biogenic silica particles included in the PCA.

Categories	Types included	Categories	Types included
Poaceae (POAC.)	All types of CRENATE, BILOBATE, POLYLOBATE, CROSS, RONDEL, ELONGATE DENDRITIC, PAPILLATE without satellites	Graminoids (GRAM.)	Those of the Poaceae and Cyperaceae categories
Cyperaceae (CYP.)	Cyperaceae PAPILLATE	Pooid (POOID)	CRENATE, RONDEL, TRAPEZIFORM SHORT CELL
BULLIFORM (Bulli)	4 types distinguished	Lobate (LO)	BILOBATE, POLYLOBATE, CROSS
Podostemaceae (PODOS.)	Podostemaceae AMOEBOID PLATE	Bambusoid Saddle (Sa-Bamb)	SADDLE > 20µ
Arecaceae (Arec.)	SPHEROID ECHINATE	Chloridoid Saddle (Sa-Chlo)	SADDLE long convex edges
Woody Dicots (WooD)	SPHEROID ORNATE	Other Saddles (Sa-o)	SADDLE collapsed, plateaued, regular
Conifers (CONI.)	4 types of BLOCKY identified	**Other biogenic silica particles:**	
Ferns (FERN)	2 types of ELONGATE	Diatoms (DIATO)	Entire valves pennate and round
Other forest indicators (FI-oth)	2 BLOCKY, 1 ELONGATE	Sponges (SPONG)	Spicules, asteroscleres, and birotulate gemmuloscleres
		Chrysophyte (CHRYSO)	Cysts

Phytolith morphotypes, which are highly redundant among plant taxa and rarely diagnostic of genus or species, were classified based on information from the literature [9-20]. Phytolith names follow the international nomenclature ICPN 2.0 [21]. Our classification, given in details in **Supplementary Information Table B2**, can be summarized as follows:

(1) Grass silica short cell phytoliths (GSSCs) are diagnostic of Poaceae. CRENATE, RONDEL, POLYLOBATE, BILOBATE, CROSS, and SADDLE morphotypes, which have been further distinguished into subtypes according to size or shape, may provide additional information [11,16], such as the morphotypes CRENATE and RONDEL with base diameter >15µ are considered markers for C_3 high-elevation grasses of the Pooideae subfamily. POLYLOBATE and *Stipa/Vossia*-type BILOBATE (short 10-18 µ BILOBATE with constriction) are considered markers of Panicoideae, while BILOBATE with scooped ends is considered a marker of Ehrhartoideae *Oryza* (mostly aquatic) grasses. Very long BILOBATE (>26 µ) with very long

shank (>7 µ) or *Aristida*-type BILOBATE is considered a marker for dry conditions. SADDLES are typical for xerophytic Chloridoideae grasses, particularly SADDLES with long convex edges (= squat saddles). Large SADDLES >20 µ mark the presence of Bambusoideae, while small CROSSES (7-10 µ) are considered markers of the aquatic *Vossia.* ELONGATE DENDRITIC phytoliths from grass inflorescences are also typical for the Poaceae family.

(2) Other morphotypes are diagnostic at family level such as SPHEROID ECHINATE for Arecaceae (palm), Cyperaceae PAPILLATE (sedges), and Podostemaceae AMOEBOID PLATE. BULLIFORM are diagnostic of Poaceae and Cyperaceae, which altogether represent Graminoid plants.

(3) Four BLOCKY morphotypes and two ELONGATE morphotypes >40 µ were recognized as originating respectively from conifers and ferns.

(4) SPHEROID ORNATE are markers for woody dicotyledons but cannot be precisely assigned taxonomically.

(5) Several other morphotypes were identified and counted separately although their taxonomical resolution is very vague, or their taxonomical origin is still unknown or uncertain.

The most common morphotypes are shown in **Supplementary Information Fig. B6**.

In productive samples, phytoliths are abundant (>60-90%) [22]. The preservation is exceptional in comparison for instance to Olduvai [23,24]. Diatoms are mainly represented by pennate forms (i.e., mainly epiphytic species), which suggests open or marshy wetland. Sponges represent up to 15% in sample 11 (archeological level D) and suggest riverine settings, also documented by the occurrence of *Podostemaceae* AMOEBOID PLATE. Siliceous *Chrysophyceae* cysts represent up to 17% of the particles in archeological level B (sample 5). They are mostly documented in Alpine and boreal to Artic environments where they occur in abundance on moss periphyton and epilithon [25], while cysts of golden-brown algae were also observed in temperate forest soils in France (DB, pers. obs.). In average, phytoliths of *Poaceae* (grasses) make up 56% and *Cyperaceae* <1% (except in Level C, 21%), while forest indicators including Conifers and woody dicots phytoliths do not exceed 22% in any assemblage (**Supplementary Information Fig. B7**). Level B (sample 5) shows greater abundance of phytoliths of conifers and ferns and of Chrysophytes, while levels C (sample 10) and D (sample 11) show more SPHEROID ORNATE (woody dicots), *Cyperaceae*, BULLIFORM, and bambusoid SADDLE phytoliths.

Principal component analysis (PCA) was carried out on percentages converted to square root to handle the high heterogeneity of the abundance data. In a first step, all identified phytolith types were considered in the analysis (67 phytolith types, plus diatoms, sponges, cysts). The most meaningful information, however, was obtained by considering Diatoms, Sponges, Chrysophytes, and a sub-set of phytolith types grouped as Poaceae, Cyperaceae, BULLIFORM, Podostemaceae, Arecaceae, Woody Dicots, Conifers, Ferns, Other Forest indicators, Graminoids, Pooid GSSCs (CRENATE + RONDEL + TRAPEZIFORM short-cell), Lobate (BILOBATES + POLYLOBATES + CROSSES), Bambusoid SADDLE type, Chloridoid SADDLE type, other SADDLE types (**Supplementary Information Table B2**).

Phytolith analysis furthermore allows making some assumption on the climate. The Ic phytolith index is a proxy of the proportions of high elevation grass species (mainly C_3) versus low elevation grass species (mainly C_4). Ic increases with increasing elevation. It somehow mirrors mean annual temperature, which is the best predictor of the proportion of C_4 grass species above atmospheric pCO_2 and precipitation [26]. Based on the phytolith index Ic calibrated on Eastern African mountains

[27], archeological levels B, C and D may have formed under cooler than present climate (**Supplementary Information Fig. B7**).

The grass phytolith assemblages are dominated by BILOBATES, including *Vossia*-type and Scooped BILOBATES, indicating that the grasslands were definitely mesophytic. They probably included a majority of C_4 grass species, but in proportions that cannot be precisely deduced from the phytoliths because phytoliths are only partially related to the photosynthetic types of grasses (**Supplementary Information Fig. B8-9**). Indeed, while the Pooid type phytoliths (CRENATE, RONDEL, TRAPEZIFORM SHORT CELL) are only produced by *Pooideae* which are exclusively C_3, the dominant morphotype in MS is BILOBATE. However, this morphotype is one of the most redundant in grasses and is found in *Ehrhartoideae* (C_3), *Bambusoideae* (C_3) *Danthonioideae* (mainly C_3) and *Panicoideae* species. In Eastern Africa about two-thirds of the latter ones are C_4 and one-third is C_3. The C_4 photosynthetic signal of BILOBATES is therefore weak [11,27]. MS paleograsslands definitely have a much more mesophytic signal compared to Olduvai (1500 m asl, 1.89-1.35 Ma). At Olduvai, phytoliths of palms (*Arecaceae*) and woody dicots exceed in abundance those of grasses (mainly RONDELS which are produced by all *Poaceae*, especially the xerophytic *Chloridoideae*).

Supplementary Information Fig. B6. Phytoliths observed in the sedimentological and archeological levels of the MS. Grass silica short cells (Poaceae) (a-d), a: Bilobate, b: Crenate, c: Polylobate, d: Saddle. e-g: Blocky morphotypes derived from woody tissues and assigned to woody dicotyledons, h: non-diagnostic Elongate that can be found in conifers and grasses, i-j: Blocky morphotypes with granular appearance typical for conifers. i: Blocky with bordered pits (arrow). Scale bar: 20 microns.

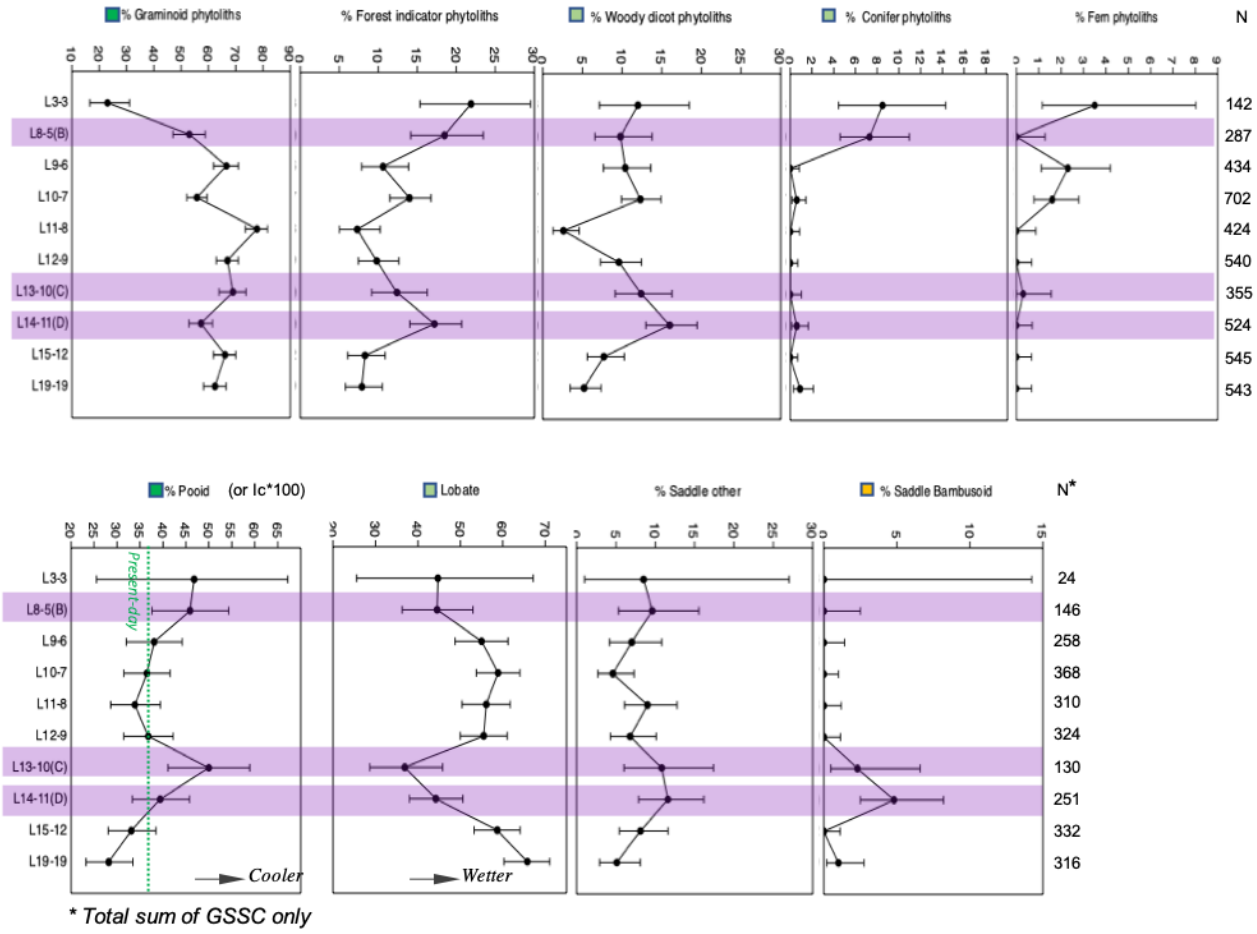

Supplementary Information Fig. B7. Plots of phytolith average relative abundance in percent, calculated on the total sum of phytoliths (N) or total sum of grass silica short cells (N*). Bars indicate 95% confidence interval. Purple shading indicates archeological samples. Graminoid include Poaceae and Cyperaceae. See **Supplementary Information Table B2** for morphotypes included in each category. Climatic index Ic is phytolith ratio of Crenate + Rondel + Trapeziform short cells/sum of grass silica short cells; calibrated on tropical East African mountains its present-day value is of about 0.35 at 2000 m [27].

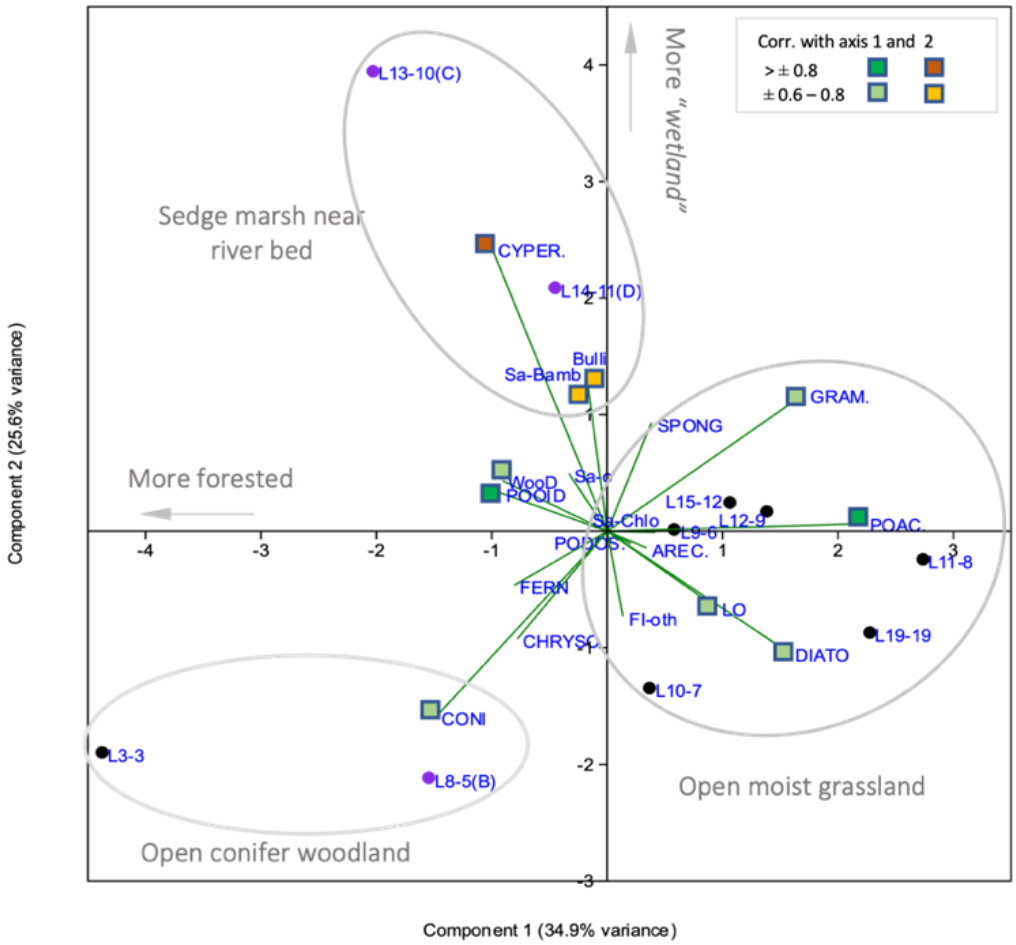

Supplementary Information Fig. B8. Principal component analysis of the MS phytolith data including only the main phytolith types. Grey circles and vegetation types were added post-hoc to the analysis and represent our interpretation. See **Supplementary Information Table B2** for phytolith morphotypes included in each category.

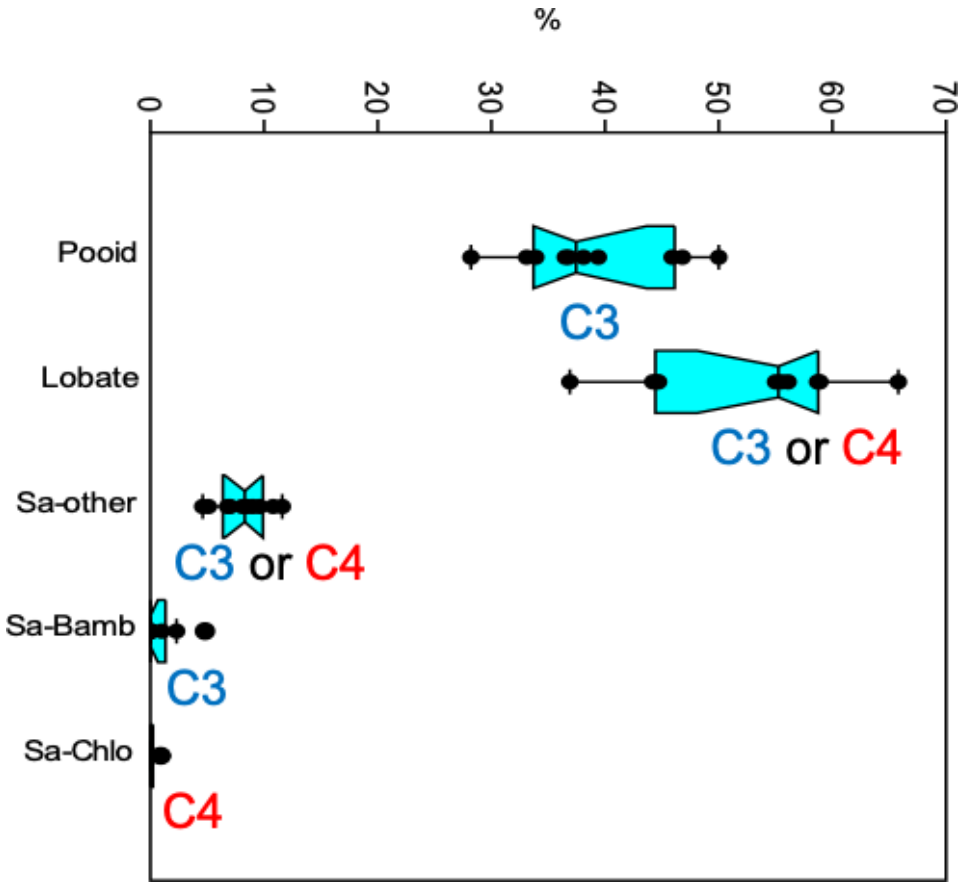

Supplementary Information Fig. B9. Box-plots showing the range for minimum and maximum values (whiskers), average, and 25-75 percent quartiles (blue boxes) of grass silica short cell phytoliths relative abundance (in %) according to their photosynthesis signal. Values were obtained from N= 10 independent sedimentological and archeological levels, Simbiro, Melka Kunture, Ethiopia. Refer to **Supplementary Information Table B2** for phytolith morphotypes included in the various categories.

Supplementary Information B3. Stable isotope analysis

Principles of carbon and oxygen isotopic tracking

Stable isotopes studies have proven useful in reconstructing aspects of paleodiet and paleoecology. The carbon and oxygen isotopic abundances in tooth enamel (carbonate apatite) of herbivores is related respectively to the types of consumed plants and to the ingested water during the formation of the analyzed tissue [28-32]

More precisely, variations in $\delta^{13}C$ values in terrestrial environments reflect the relative abundance of C_3 and C_4 plants, following the two main photosynthetic pathways. C_3 plants consist of trees, herbaceous plants, cool-season grasses and have $\delta^{13}C$ values ranging from -35‰ to -20‰ (mean -27‰). C_4 plants include many grass species and sedges in tropical areas and have $\delta^{13}C$ values ranging from -14‰ to -9‰ (mean -12‰) [33-35]. Oxygen isotopic ($\delta^{18}O$) abundance reflects the source and amount of body-water ingested through plants or drinking water. Many factors play a relevant role in the change of oxygen isotopic composition, as the continental effect, amount effect, latitude, precipitations, and temperature [36-40].

Furthermore, mammal water-dependent drinkers usually have lower $\delta^{18}O$ values lower than non-obligate drinkers, depending on water availability and rainfall seasonality. Oxygen isotopic composition can also be affected by habitat differences: for aquatic or water-dependent mammals such as hippos, stable oxygen isotopes are depleted compared to terrestrial herbivores [32,36,41].

Materials and methods

The measurements of $^{13}C/^{12}C$ and $^{18}O/^{16}O$ isotopic ratios were performed on 14 fossil teeth representing a range of taxa identified at the family level (hippopotamids, equids, and bovids) from several archeological levels (A, n=7; B, n=11; D, n=7. Suitable fossil teeth were not available in Level C (**Supplementary Information Table B3**).

The samples have been collected at the National Museum of Ethiopia (Addis Ababa), in agreement with the ARCCH (Authority for Research and Conservation of the Cultural Heritage) authorities and with Prof. Margherita Mussi, director of the Italo-Spanish archaeological mission at Melka Kunture and Balchit (Ethiopia).

Fossil enamel was sampled using a drilling device equipped with a diamond-tipped bit to obtain 12-15 mg of powder. For the analysis, we took bulk and intra-tooth samples. The bulk sampling technique consists in engraving a vertical line on the tooth, to obtain a mean estimate of the individual's diet during the period of tooth formation, averaging any seasonal fluctuation in isotopic ratios. In contrast, intra-tooth serial sampling allows isotopic measurements from different periods of an individual's life. Samples are taken drilling horizontal bands and perpendicularly to the growth axis of the tooth [42].

Enamel powder pre-treatment and isotopic analysis were conducted at the Biogeology Unit of the Geoscience Department at the University of Tübingen (Germany). Powdered samples were soaked in 2–3% NaOCl for 24h at 20°C to oxidize organic residues and rinsed twice with distilled water. Then the remaining samples were treated with 0.1 M buffer acetic acid-calcium acetate (pH = 4.66) for 24h at 20°C to remove exogenous carbonate [36]. The international reference standards are "Vienna PeeDee Belemnite" (VPDB) for the carbon and oxygen and "Vienna Standard Mean Ocean Water" (VSMOW) for oxygen. Stable isotopic results are expressed in the following standard δ-notations: $X = [(R_{sample}/R_{standard})-1]^{*}1000$, where X is referred to $\delta^{13}C$ and $\delta^{18}O$ values and R represent $^{13}C/^{12}C$ or $^{18}O/^{16}O$, respectively. Pretreated (sample/enamel) carbonate was reacted with 99% H_3PO_4 for 4 h at 70 °C using a MultiFlow-Geo interfaced with the Elementar IsoPrime 100 IRMS. Final isotopic ratios are reported per mil (‰) calibrated with international standards (IAEA-603: $\delta^{13}C$ = 2.46 / $\delta^{18}O$ = -2.37 and NBS-18: $\delta^{13}C$ = -5.014 / $\delta^{18}O$ = -23.2), as well as three in-

house standards. IonOS software (Version 4.3) by Elementar was used to carry out multi-point standard isotope calibration by generating a trend line (y=mx+c) that maps measured versus expected isotopic results, which is then used to calibrate sample results [43-45]

Intra-tooth variation analysis

The Simbiro isotopic results ($\delta^{13}C$ and $\delta^{18}O$) were compared to similar data published by Souron *et al*. [42]. In this study, the authors applied a high-resolution tooth enamel serial sampling (one sample every 1mm to 3mm) on a lower (MA06-04 Ci) and an upper (MA06-04 Cs) canine of a single common *Hippopotamus* from the Chari River, southern Chad. Authors also used the same protocol for two fossil specimens of the Shungura Formation, an aff. *Hippopotamus protamphibius turkanensis* (OMO 112/2-10014) and an aff. *Hippopotamus protamphibius protamphibius* (OMO 331-10003) [42]. The Shungura Formation is located in the Lower Omo Valley (south-western Ethiopia), at ~638 m a.s.l. It is one of the most complete Plio-Pleistocene continental sequences, with ca. 800 m of interstratified volcanic tuffs, fluviatile, and fluvio-lacustrine sediments deposited between ~3.6 Ma and ~1.0 Ma [46,47]. More precisely, OMO 112/2-10014 and OMO 331-10003 were unearthed from units B-9 and C-9, from deposits a few meters below dated $^{40}Ar/^{39}Ar$ levels [48]: B-10-1 (2.965 ± 0.014 Ma) and Tuff D (2.526 ± 0.014 Ma), respectively.

Souron *et al*. [42] took samples at linear intervals of 1-3mm, while we did the same at intervals of c. 5mm. Furthermore, Souron *et al*. [42] analyzed 20 to 41 samples from each modern or fossil specimen, while we took 9 samples altogether from tooth n° 2056 discovered in the MS. In order to allow all the same a comparison, we plotted the isotopic data from Souron *et al*. [42] samples considering only those at c. 5mm from each other and ignoring those in between. This simulated greater distance between sampling spots makes easier any comparison with our own results and also reduced the data number by around half.

Reducing the sampling resolution and the number of samples, we made scatter graphs which compare intra-tooth data by Souron *et al*. [42] with the hippo tusk n° 2056 (**Supplementary Information Fig. B11**). Extant hippos produced $\delta^{13}C$ and $\delta^{18}O$ values with greater variation than the fossil ones, even if in the MS specimen the values range is less variable than in those of Souron *et al*. [42].

In conclusion, intra-tooth values from the hippo tusk of the MS show a clear consumption of C_4 plants and a stable trend in the diet and water source. Furthermore, as the teeth from the MS and from the Shungura Formation were all deposited in fluvial sediments, a fluvial habitat can be reasonably inferred, even taking into account transport and redeposition by a flowing river. Comparisons with Souron *et al*. [42] results are useful to properly understand seasonal variations during the lifetime of a fossil hippo. However, more specimens and sampling at higher resolution are both needed to confirm that the stable trend observed in hippo tooth n° 2056 actually reflects a general pattern and can be considered, as such, a reliable paleoenvironmental signal.

Interpretation

The $\delta^{13}C$ values of hippopotamids range from -0.8‰ to +2.1‰, pointing to a C_4 diet, with only a single value (-2.4‰) that could be interpreted as a C_3/C_4-mixed diet indicator. The $\delta^{13}C$ values of bovids and equids (all of them terrestrial herbivores and therefore grouped in the same category) range from +0.16‰ to +4.2‰ (**Supplementary Information Fig. B10**). Thus, the $\delta^{13}C$ values from the MS measured through bulk sampling on hippopotamids, bovids, and equids are all indicative of the consumption of C_4 plants, pointing to a grassland. However, hippopotamids seem to be more versatile, including a low amount of C_3 plants in their diet, as observed at other African sites [41,49].

The $\delta^{18}O$ values of hippopotamids show values ranging from +18.9‰ to +23.9‰, while the values of bovids and equids range from +22.2‰ to +28.2‰ (**Supplementary Information Fig. B10**). The

oxygen data confirm a well-known isotopic feature of hippopotamids, which consistently show $\delta^{18}O$ values lower than those of terrestrial herbivores. This is linked to the distinction between semiaquatic and terrestrial habitats [32,36].

The intratooth method was applied on a fragment of *Hippopotamus* cf. *amphibius* tusk (**Supplementary Information Fig. B11-12**) from level B. Enamel bioapatite $\delta^{13}C$ values vary from -2.2‰ to -0.9‰, while $\delta^{18}O$ values range from +18.0‰ to +19.7‰. Intratooth analyses show uniform isotopic results with no significant variation in either $\delta^{13}C$ or $\delta^{18}O$. This indicates a stable C_4 diet and water conditions during tusk growth (**Supplementary Information Fig. B13**).

Supplementary Information Table B3. Isotopic results from the fossil teeth of the MS.

ID code	Site	Level	Taxon	Tecnique	Tissue	$\delta^{13}C_{VPDB}$	$\delta^{18}O_{VSMOW}$
MLK-36	MS	A	*Hippopotamus* cf. *amphibius*	bulk sampling	enamel	+2.1	+23.9
MLK-10	MS	A	*Equidae*	bulk sampling	enamel	+3.1	+28.2
MLK-12	MS	A	*Equidae*	bulk sampling	enamel	+2.1	+23.1
MLK-85	MS	A	*Bovidae (Alcelaphini)*	bulk sampling	enamel	+4.2	+25.3
MLK-86	MS	A	*Bovidae*	bulk sampling	enamel	+0.83	+23.6
MLK-88	MS	A	*Bovidae*	bulk sampling	enamel	+2.7	+23.3
MLK-37	MS	A	*Bovidae*	bulk sampling	enamel	+0.16	+22.2
MLK-30	MS	B	*Hippopotamus* cf. *amphibius*	bulk sampling	enamel	-1.7	+18.9
MLK-9	MS	B	*Hippopotamus* cf. *amphibius*	bulk sampling	enamel	-2.4	+21.1
MLK-38	MS	B	*Hippopotamus* cf. *amphibius*	serial sampling	enamel	-1.8	+18.0
MLK-39	MS	B	*Hippopotamus* cf. *amphibius*	serial sampling	enamel	-2.1	+18.2
MLK-40	MS	B	*Hippopotamus* cf. *amphibius*	serial sampling	enamel	-2.2	+19.1
MLK-41	MS	B	*Hippopotamus* cf. *amphibius*	serial sampling	enamel	-1.6	+19.3
MLK-42	MS	B	*Hippopotamus* cf. *amphibius*	serial sampling	enamel	-1.5	+19.3
MLK-43	MS	B	*Hippopotamus* cf. *amphibius*	serial sampling	enamel	-1.1	+19.4
MLK-44	MS	B	*Hippopotamus* cf. *amphibius*	serial sampling	enamel	-0.9	+19.3
MLK-45	MS	B	*Hippopotamus* cf. *amphibius*	serial sampling	enamel	-1.4	+19.6

MLK-46	MS	B	*Hippopotamus* cf. *amphibius*	serial sampling	enamel	-1.4	+19.7
MLK-28	MS	E	*Hippopotamus* cf. *amphibius*	bulk sampling	enamel	-0.8	+22.2
MLK-29	MS	E	*Hippopotamus* cf. *amphibius*	bulk sampling	enamel	+0.18	+22.9
MLK-31	MS	E	*Hippopotamus* cf. *amphibius*	bulk sampling	enamel	-0.4	+23.8
MLK-95	MS	E	*Bovidae (Hippotragini)*	bulk sampling	enamel	+2.1	+24.4
MLK-97	MS	E	*Bovidae*	bulk sampling	enamel	+3.5	+25.9
MLK-98	MS	E	*Bovidae*	bulk sampling	enamel	+3.6	+26.8
MLK-99	MS	E	*Bovidae*	bulk sampling	enamel	+3.4	+26.7

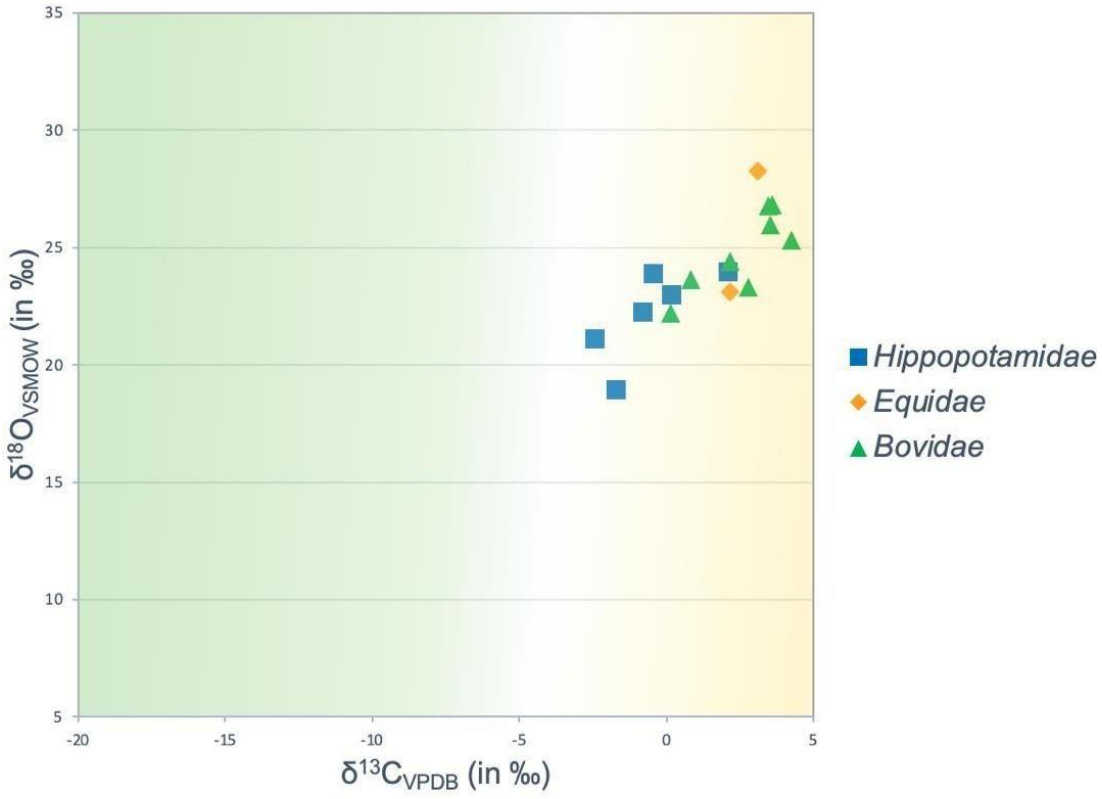

Supplementary Information Fig. B10. Bivariate plot of $\delta^{13}C$ and $\delta^{18}O$ values (enamel) for the faunal specimens from MS of Simbiro III. Green, white, and yellow shades indicate C_3, mixed C_3-C_4, and C_4 diets, respectively.

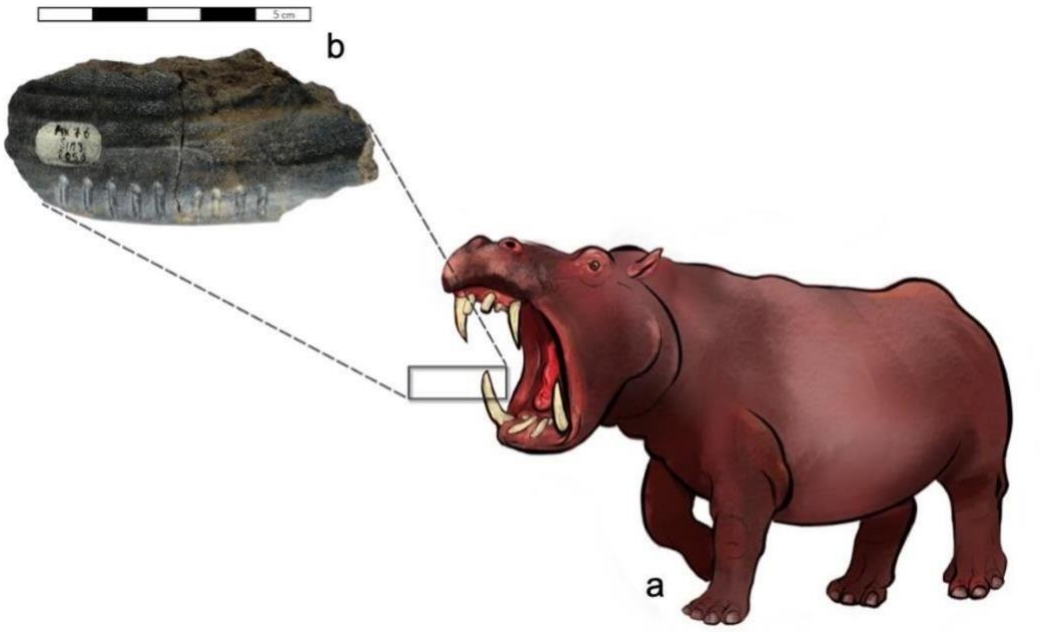

Supplementary Information Fig. B11. Sampled hippo tooth**:** a: illustration of a hippo; b: photo detail of the tusk fragment n° 2056 sampled for intra-tooth analysis.

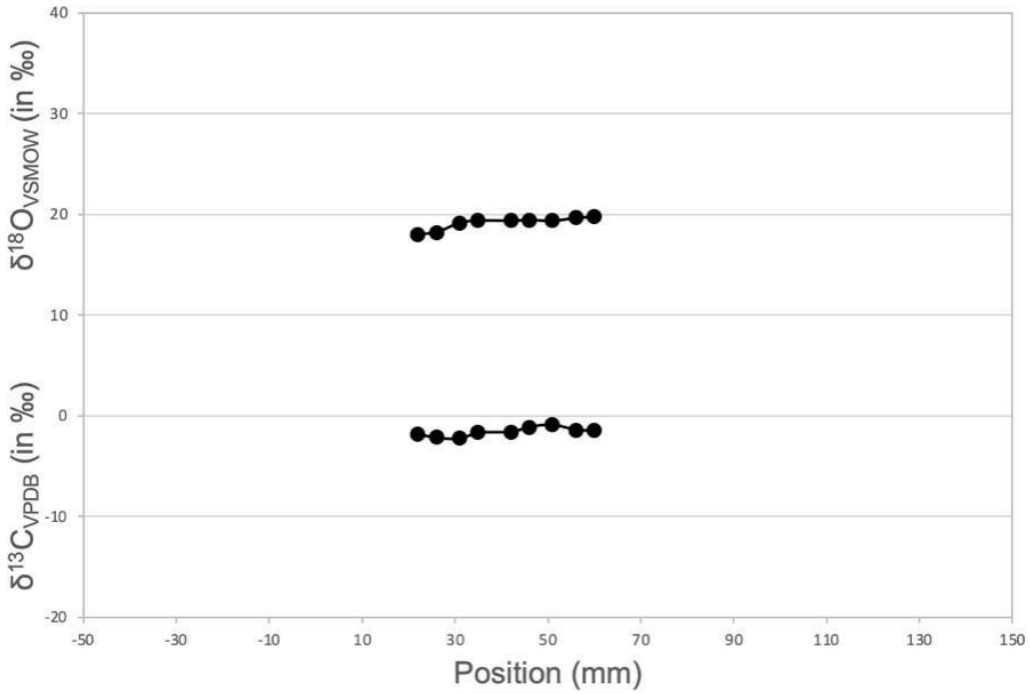

Supplementary Information Fig. B12. Plot of $\delta^{13}C$ and $\delta^{18}O$ intra-tooth values (enamel) measured along the hippo tusk fragment n° 2056 of the MS.

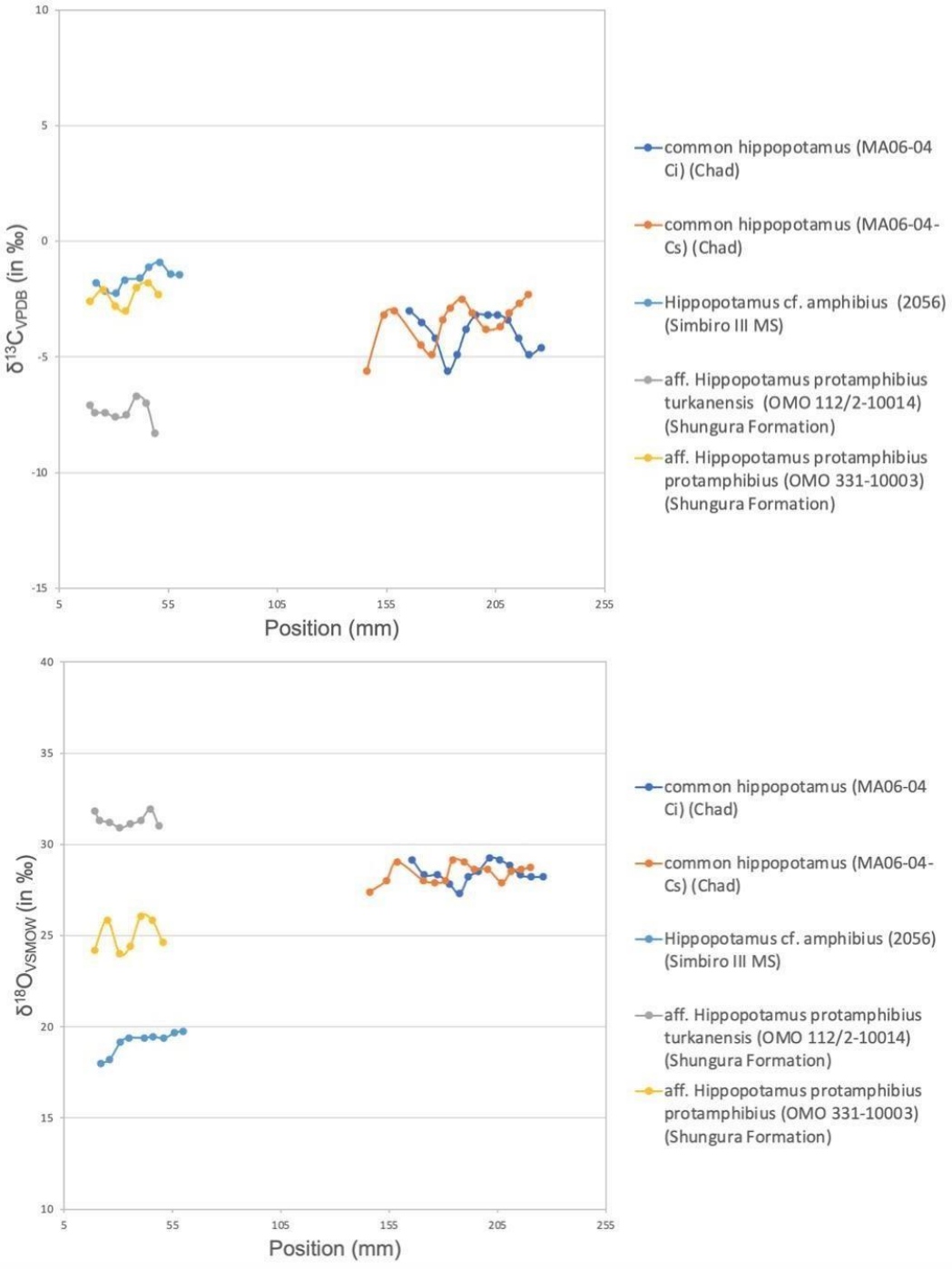

Supplementary Information Fig. B13. Plot of $\delta^{13}C$ and $\delta^{18}O$ intra-tooth values (enamel) measured along the following teeth: the lower (MA06-04 Ci) and upper canine (MA06-04 Cs) of a common *hippopotamus* from Chad[42]; a fragmented tusk of *Hippopotamus cf. amphibius* (ID 2056) from the MS of Simbiro III (this study); an aff. *Hippopotamus protamphibius turkanensis* (OMO 112/2- 10014) and an aff. *Hippopotamus protamphibius protamphibius* (OMO 331-10003) from the Shungura Formation[42].

Supplementary Information C. The archeological record

After the inventory made by Chavaillon and kept in the archives of the archeological mission, the excavated lithic assemblage totals 1474 pieces (level A = 211, level B: 636, level C = 507, level D = 13 and level E = 107) (**Supplementary Information Fig. C1**). We added 70 pieces from Piperno's fieldwork in level C and 12 eroding pieces recovered during the current stratigraphic research at the MS section.

The artefact assemblage of level A is approximately half on coarse volcanic rocks (52.1%) and half on obsidian (47.9%). We identify hammerstones, flakes, cores, retouched flakes, a single handaxe and choppers. The lithic industry of level B is knapped mostly on coarse volcanic rocks (81.7%), with the obsidian markedly less frequent (18.3%). The assemblage includes a substantial percentage of flakes but large cutting tools (LCTs) (**Supplementary Information Fig. C2)** and large flakes are prevalent. Cores and other types of artifacts are less well represented. The artifacts recovered from level D are few and actually not representative. Note the existence of various Acheulean LCTs, including a handaxe and a cleaver on flake (**Supplementary Information Fig. C3)**. The analyzed assemblage from level E includes a large number of tools on coarse volcanic rocks (61.4%) and a smaller number on obsidian (38.6%). We identified a substantial number of cores and small-medium flakes. Other techno-types are flake tools, large flakes, and LCTs (**Supplementary Information Fig. C4)**.

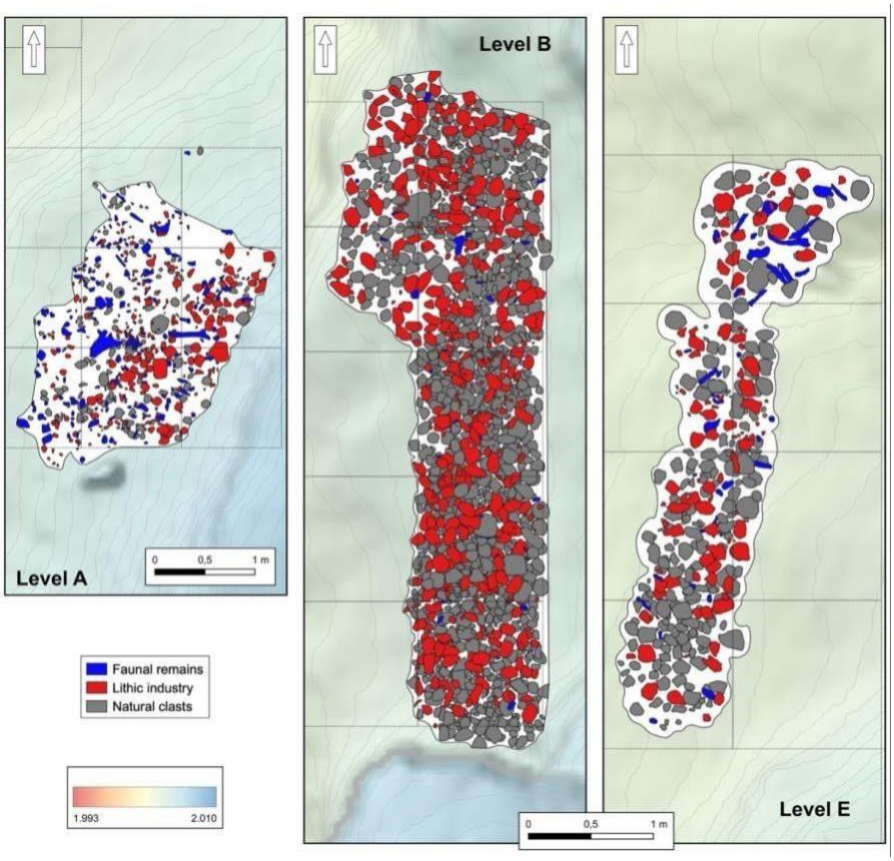

Supplementary Information Fig. C1. Plans of levels A, B and E by type of remain.

Supplementary Information Fig. C2. Level B: handaxes (1-2) and a knife (3).

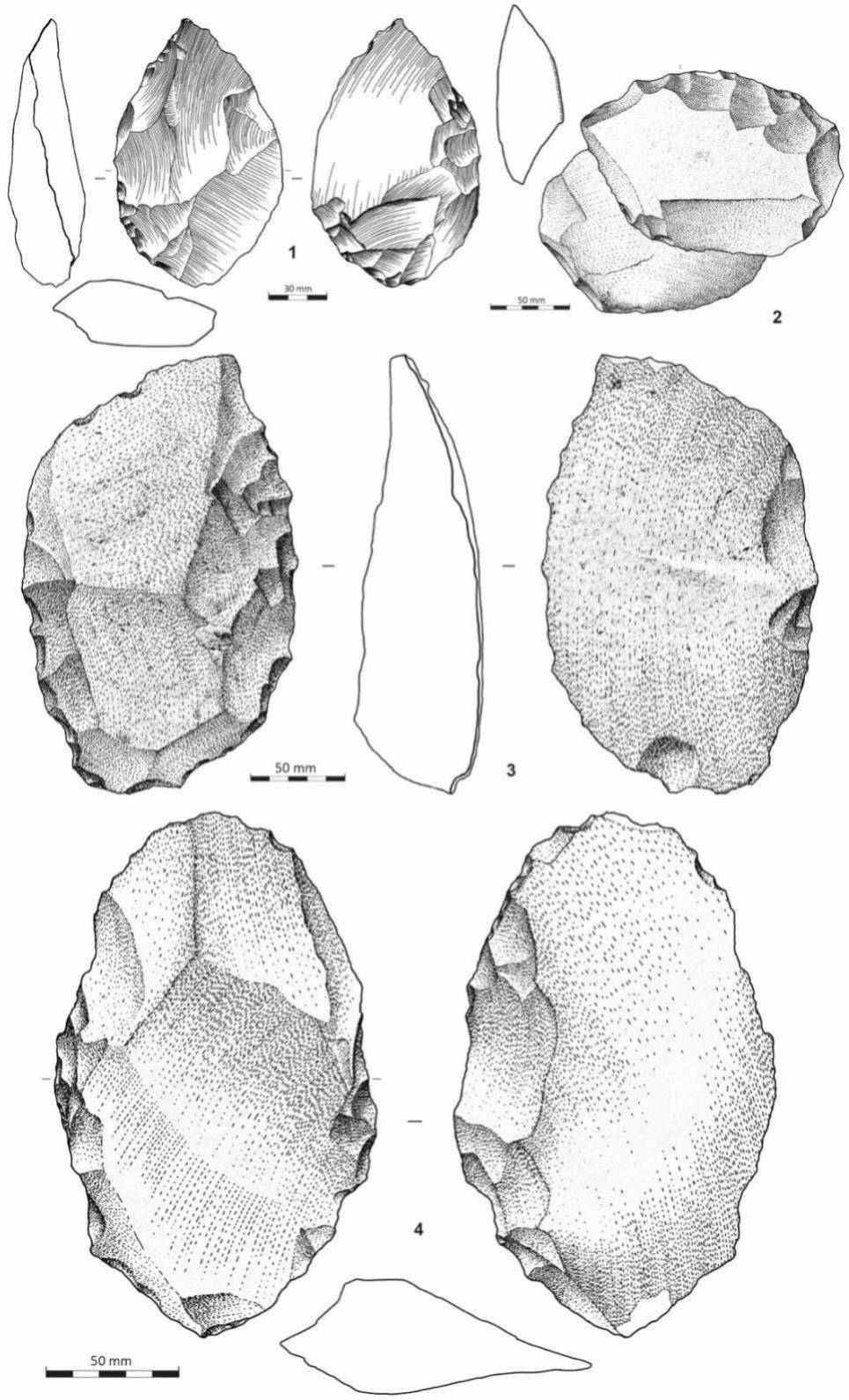

Supplementary Information Fig. C3. Level D: obsidian partial handaxe (1), massive obsidian scraper (2), basalt flake cleaver (3), basalt flake (4).

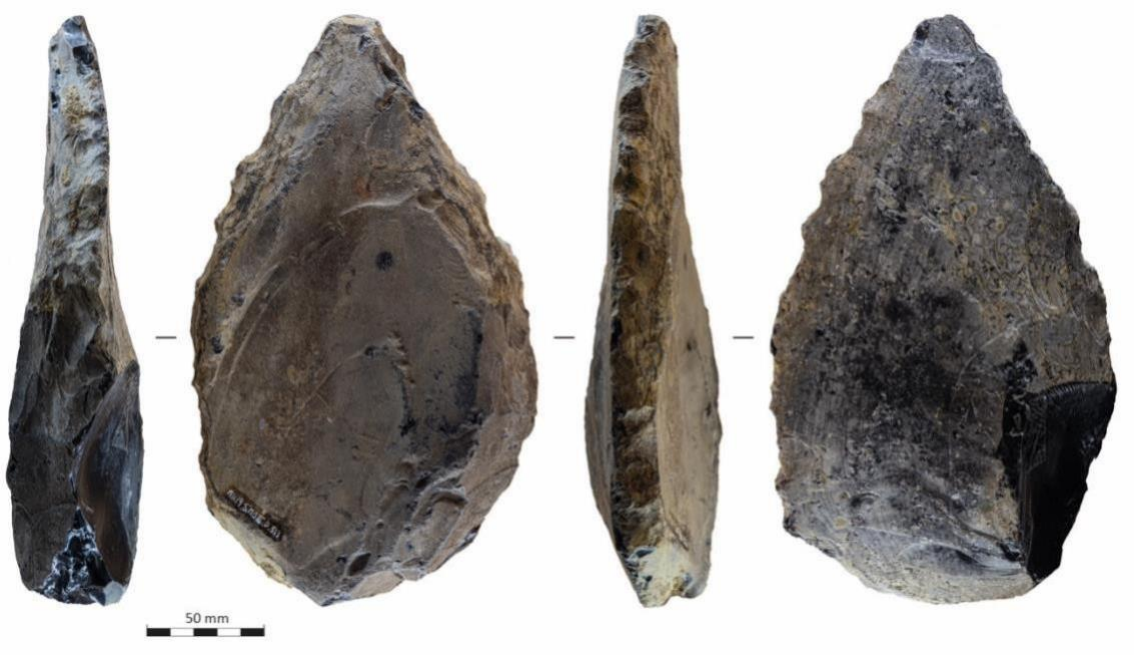

Supplementary Information Fig. C4. Level E: large partial handaxe on an obsidian flake.

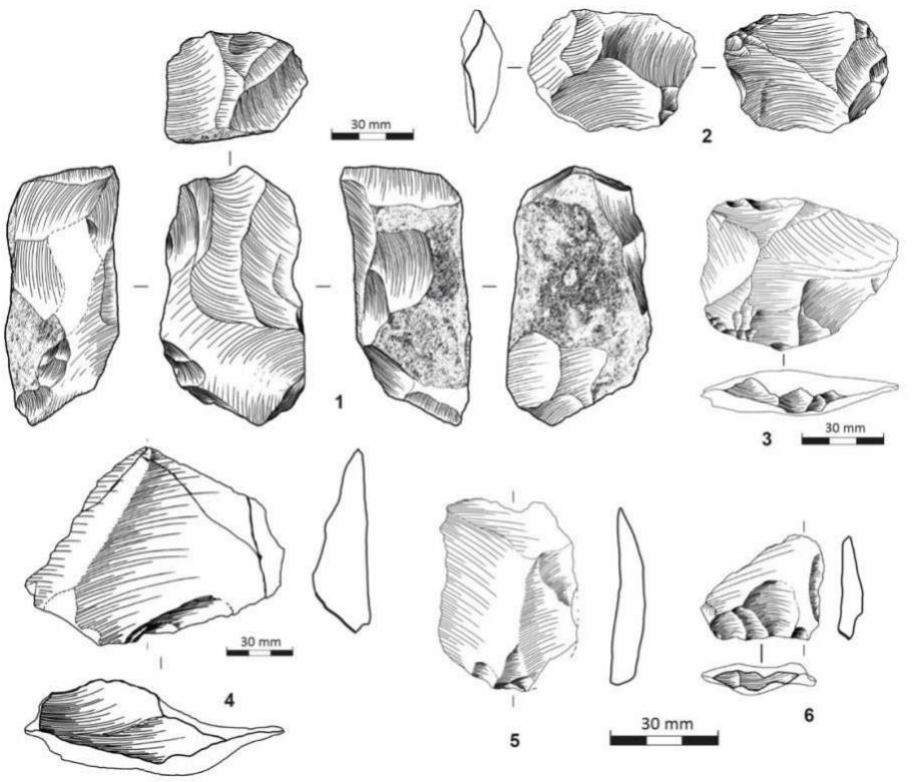

Supplementary Information Fig. C5. Level C: obsidian cores (1-2) and LCTs shaping flakes (3-6).

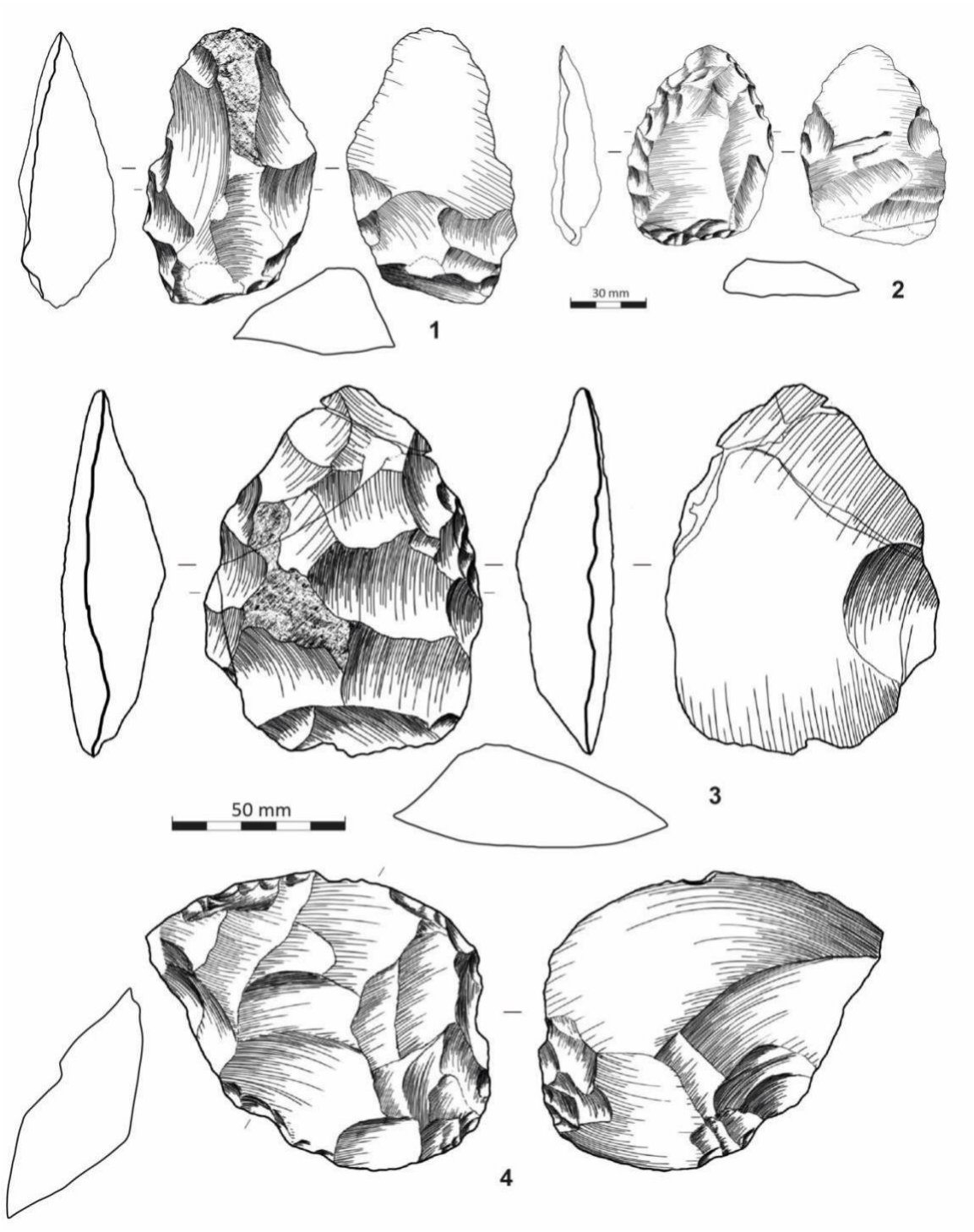

Supplementary Information Fig. C6. Level C: some examples of obsidian flake tools.

Site	*n*	Range	Average	SD
Garba I	4435	11-272	63,5	45,1
Gombore II	637	50-270	91,4	35,4
MS-level B	435	17-230	91,6	49,3
MS-level C	533	8-124	42,9	18,7

Supplementary Information Table C1. The size of artefact from various Acheulean assemblages of Melka Kunture

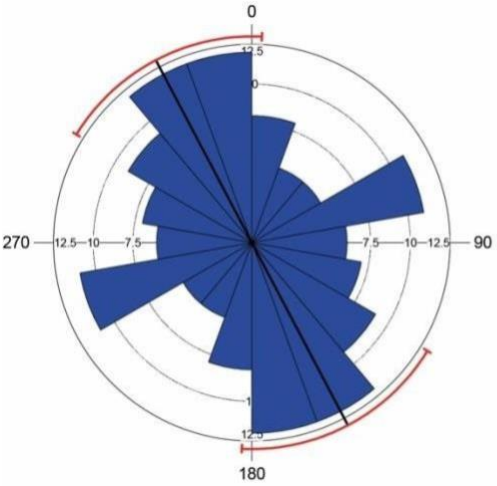

Number of Observations	75
Mean Vector (μ)	152.223°
Length of Mean Vector (r)	0.149
Concentration	0.302
Circular Variance	0.425
Circular Standard Deviation	55.891°
Rayleigh Test (Z)	1.667
Rayleigh Test (p)	0.189
Kuiper's Test (Uniform, V)	1.756
Kuiper's Test (p)	< 0.05

Supplementary Information Fig. C7. Rose diagram and calculated orientation values of artifacts from level C

Without Jackknifed									
Site	**Level C**	**Level B**	**Atebella**	**Garba I**	**Langano lake**	**Garba XIII**	**Gombore II OBS**	**Gombore II**	**Total**
MS_Level C	100,0	0,0	0,0	0,0	0,0	0,0	0,0	0,0	16
MS_Level B	3,4	86,2	0,0	0,0	6,9	3,4	0,0	0,0	29
Atebella	0,0	0,0	100,0	0,0	0,0	0,0	0,0	0,0	4
Garba I	0,0	11,1	0,0	88,9	0,0	0,0	0,0	0,0	9
Langano lake	0,0	0,0	0,0	0,0	100,0	0,0	0,0	0,0	5
Garba XIII	0,0	0,0	0,0	0,0	0,0	100,0	0,0	0,0	6
Gombore II OBS	0,0	0,0	0,0	0,0	0,0	0,0	100,0	0,0	36
Gombore II	0,0	3,2	0,0	0,0	0,0	0,0	3,2	93,5	31
Total	17	27	4	8	7	7	37	29	136
With Jackknifed									
Site	**Level C**	**Level B**	**Atebella**	**Garba I**	**Langano lake**	**Garba XIII**	**Gombore II OBS**	**Gombore II**	**Total**
MS_Level C	50,0	37,5	0,0	6,3	6,3	0,0	0,0	0,0	16
MS_Level B	17,2	41,4	6,9	10,3	10,3	6,9	3,4	3,4	29
Atebella	0,0	50,0	0,0	50,0	0,0	0,0	0,0	0,0	4
Garba I	22,2	33,3	0,0	22,2	0,0	0,0	22,2	0,0	9
Langano lake	0,0	40,0	0,0	20,0	40,0	0,0	0,0	0,0	5
Garba XIII	0,0	33,3	0,0	0,0	16,7	33,3	0,0	16,7	6
Gombore II (obsidian)	2,8	2,8	2,8	11,1	5,6	0,0	50,0	25,0	36
Gombore II	3,2	0,0	3,2	3,2	3,2	9,7	16,1	61,3	31
Total	17	27	4	8	7	7	37	29	136

Supplementary Information Table C2. Confusion matrix on the GPA data of the handaxes in the analysed samples.

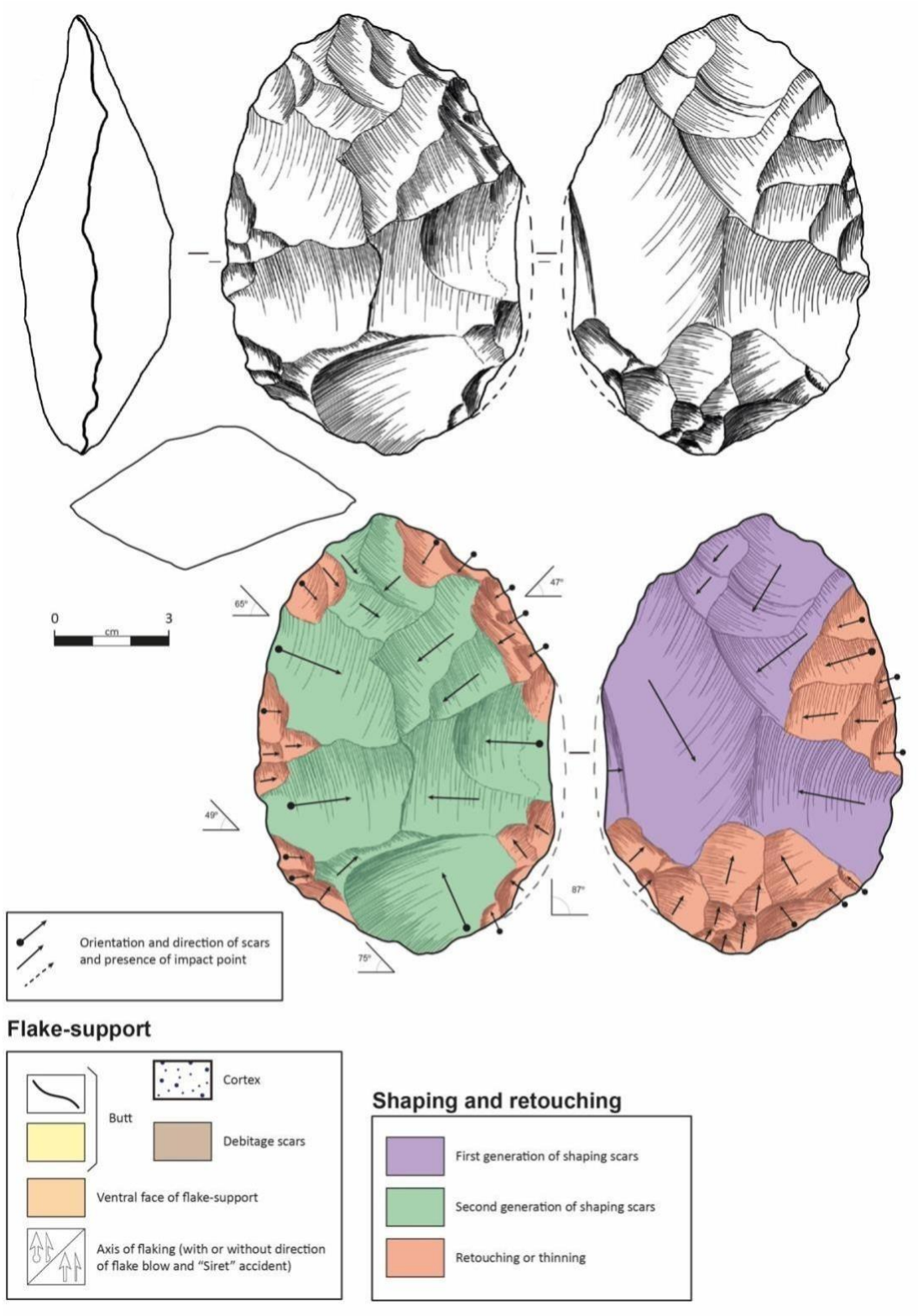

Supplementary Information Fig. C8. Level C: obsidian handaxe on an indeterminate blank with full bifacial reduction.

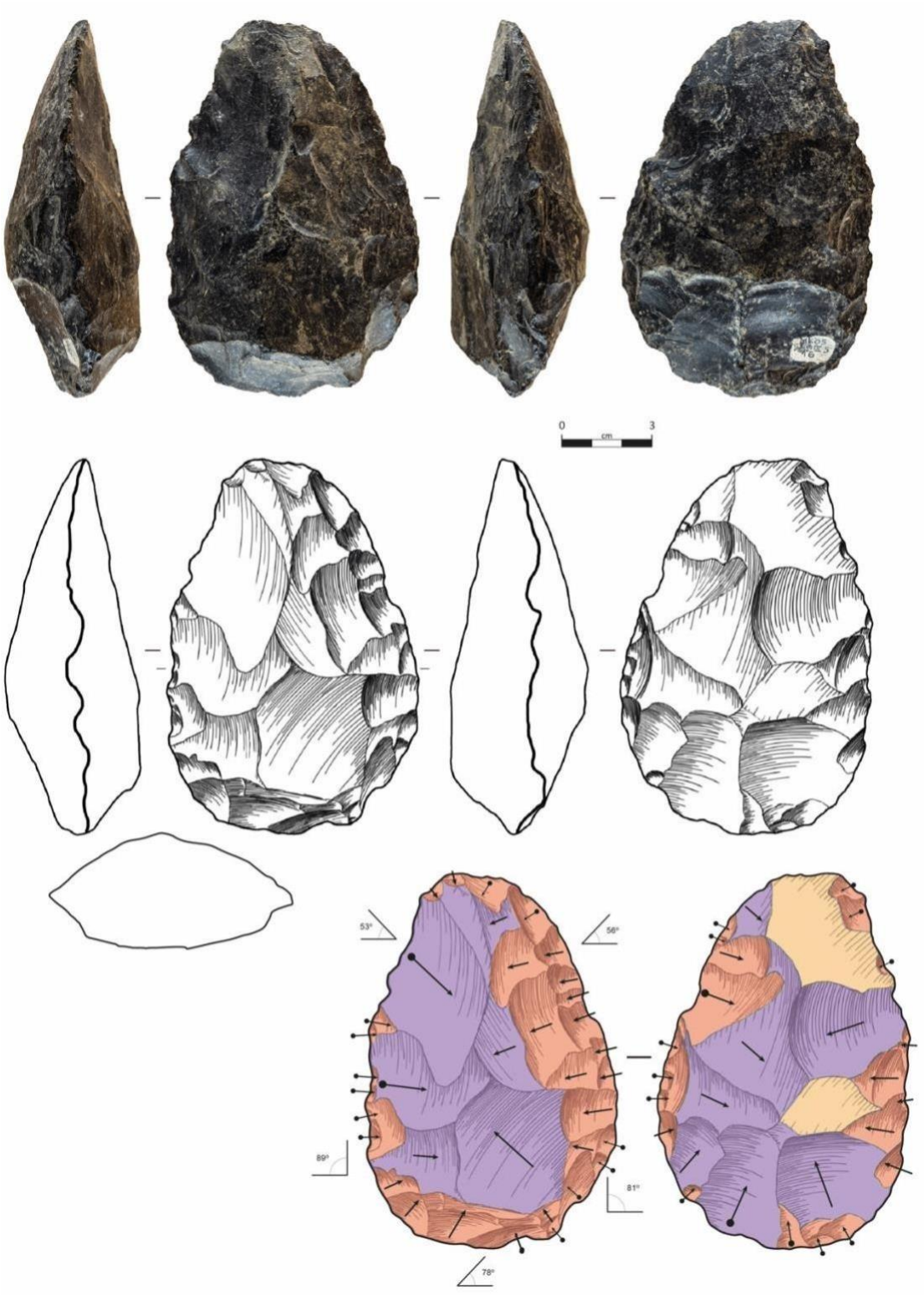

Supplementary Information Fig. C9. Level C: obsidian handaxe with full bifacial reduction on an indeterminate blank.

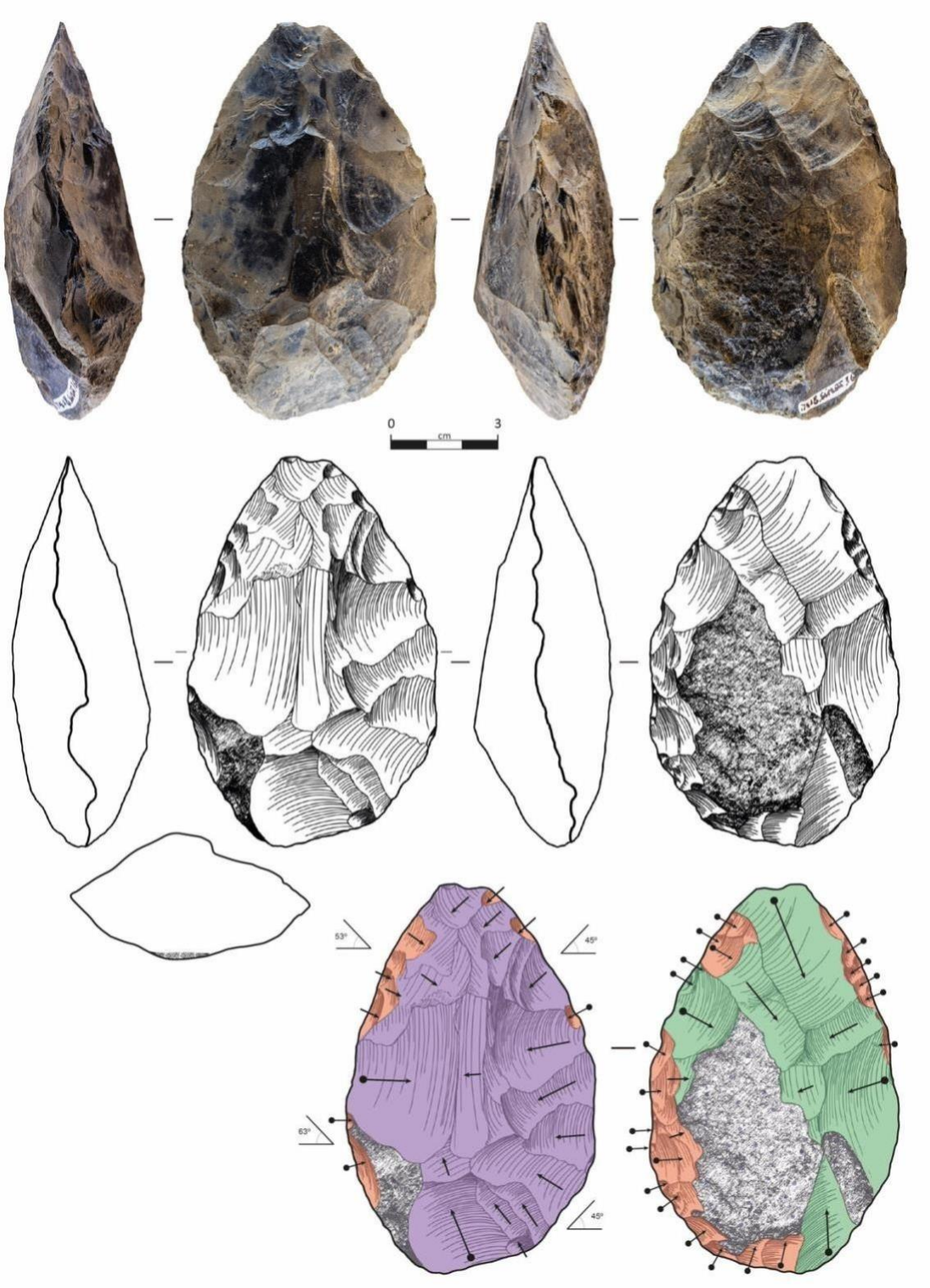

Supplementary Information Fig. C10. Level C: handaxe on an obsidian pebble with full bifacial reduction.

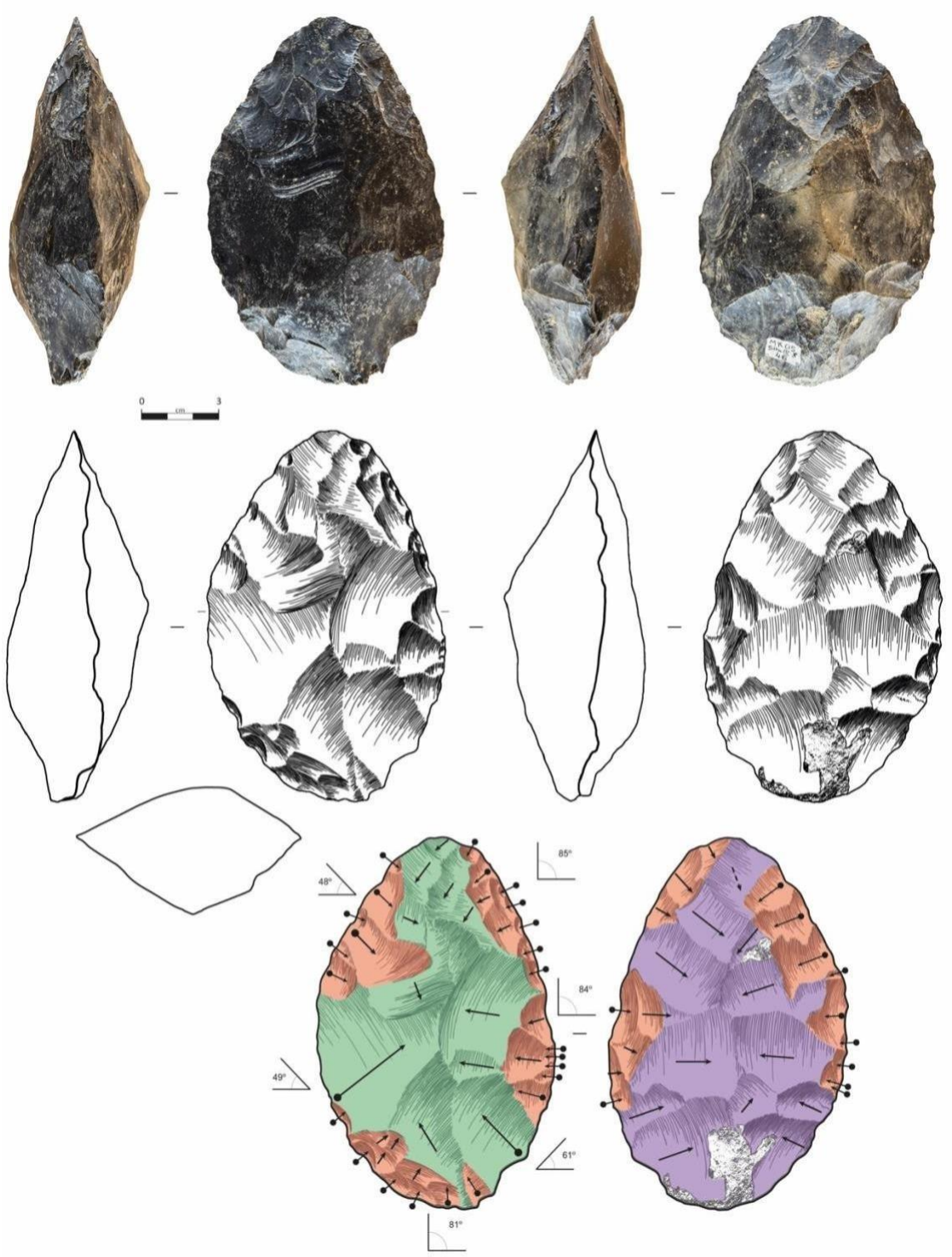

Supplementary Information Fig. C11. Level C: obsidian handaxe on an indeterminate blank with full bifacial reduction.

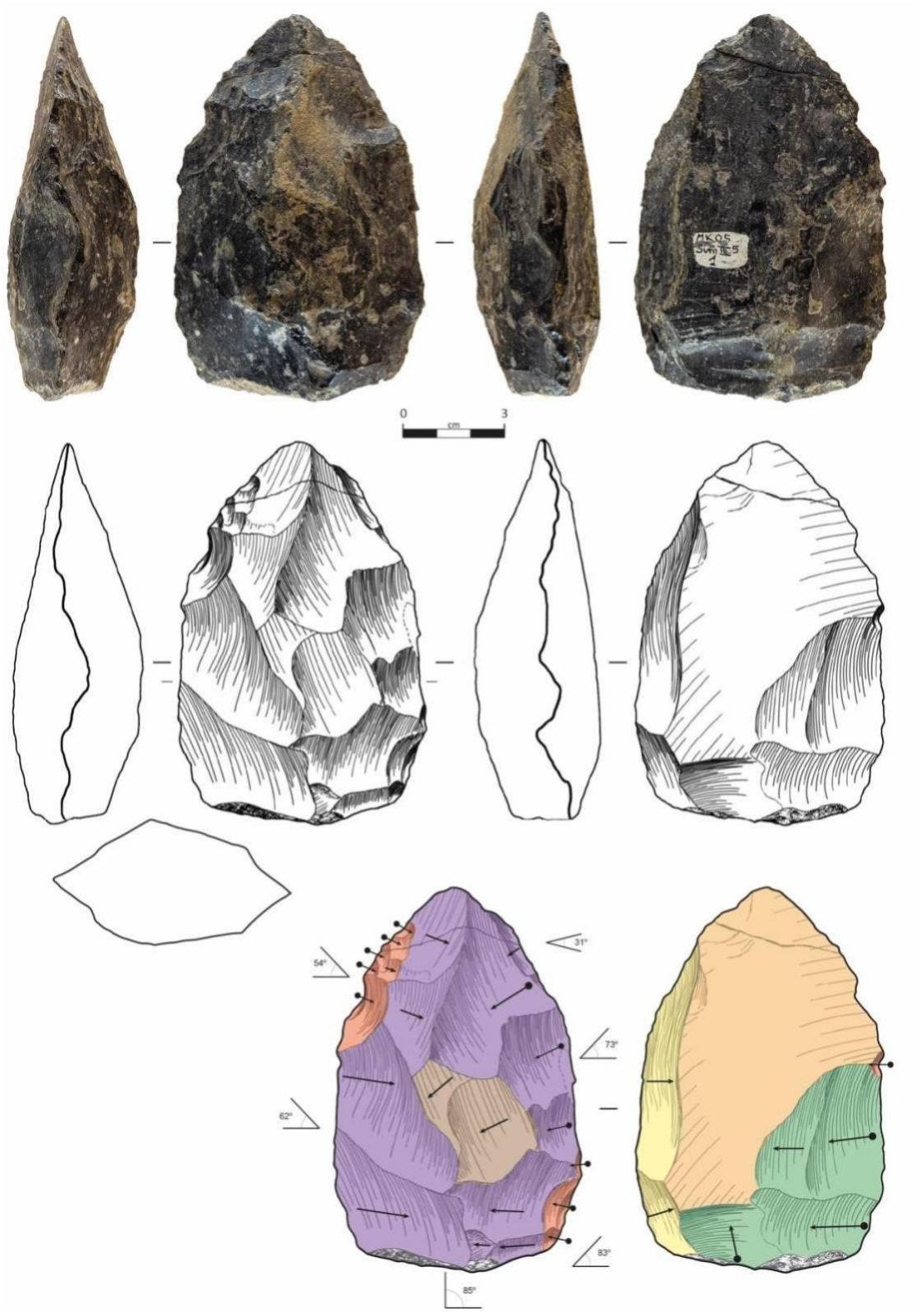

Supplementary Information Fig. C12. Level C: obsidian handaxe on an indeterminate flake with partial bifacial reduction.

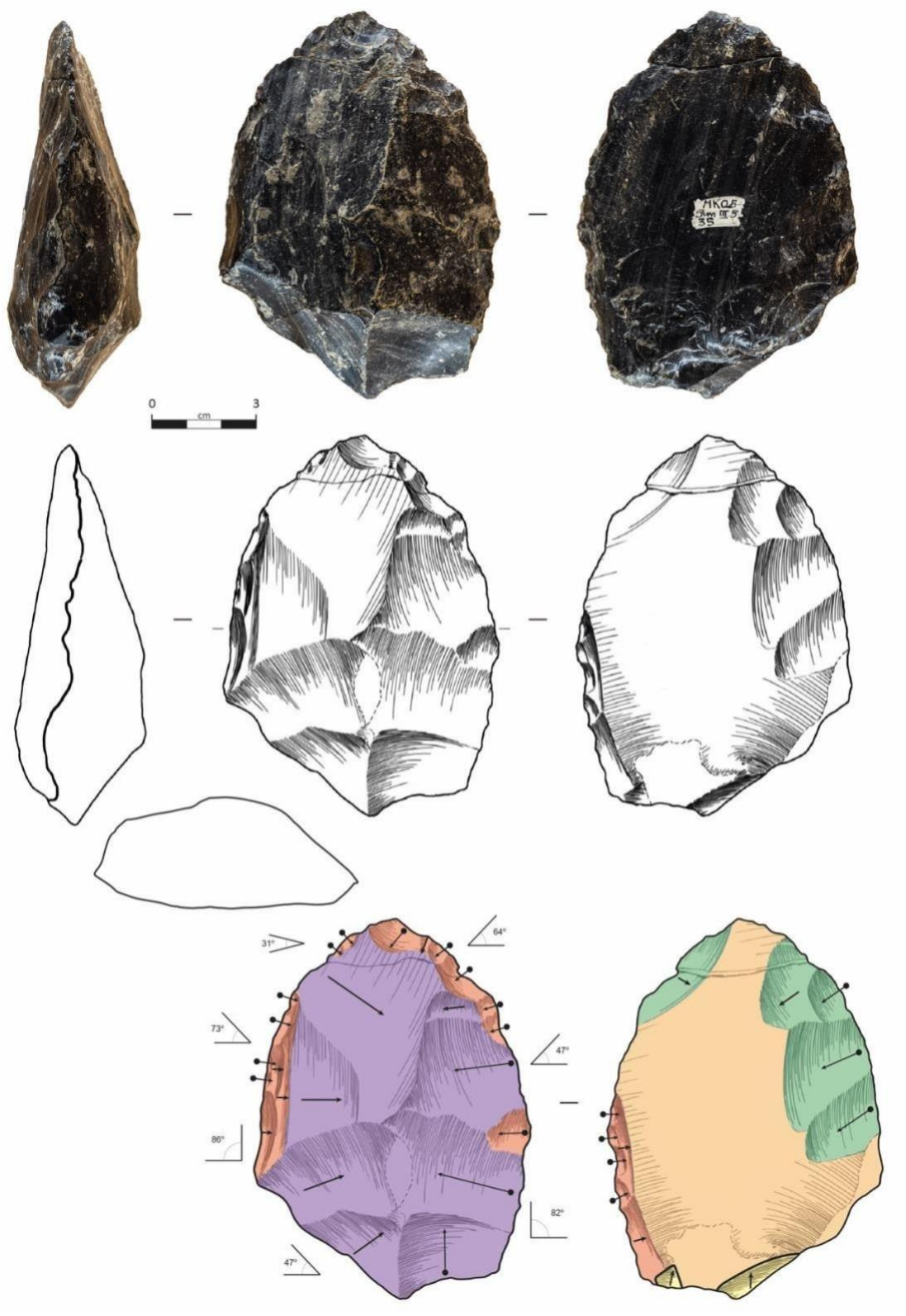

Supplementary Information Fig. C13. Level C: obsidian handaxe on an indeterminate flake with partial bifacial reduction.

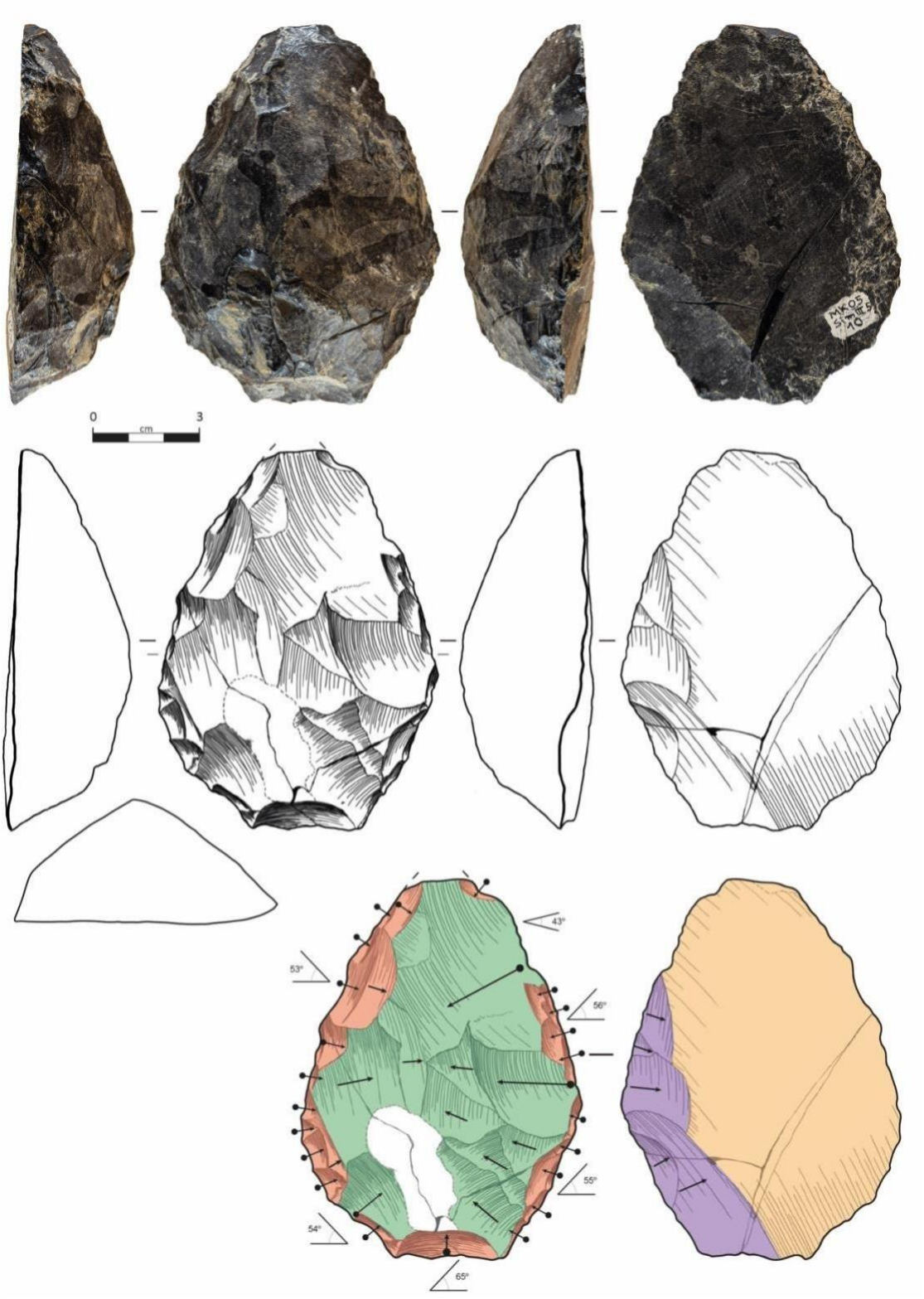

Supplementary Information Fig. C14. Level C: obsidian handaxe on an indeterminate flake with partial bifacial reduction.

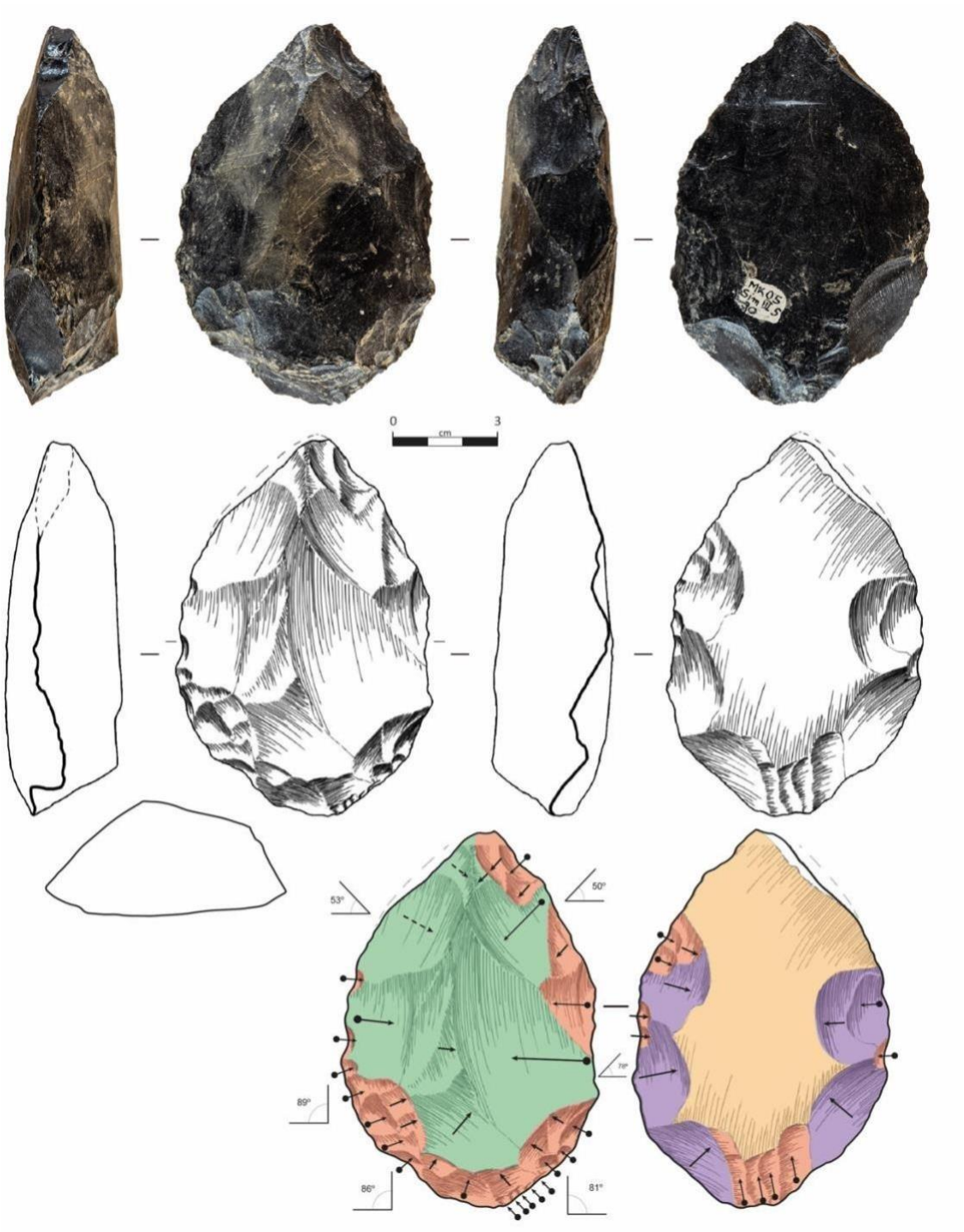

Supplementary Information Fig. C15. Level C: obsidian handaxe on an indeterminate flake with partial bifacial reduction.

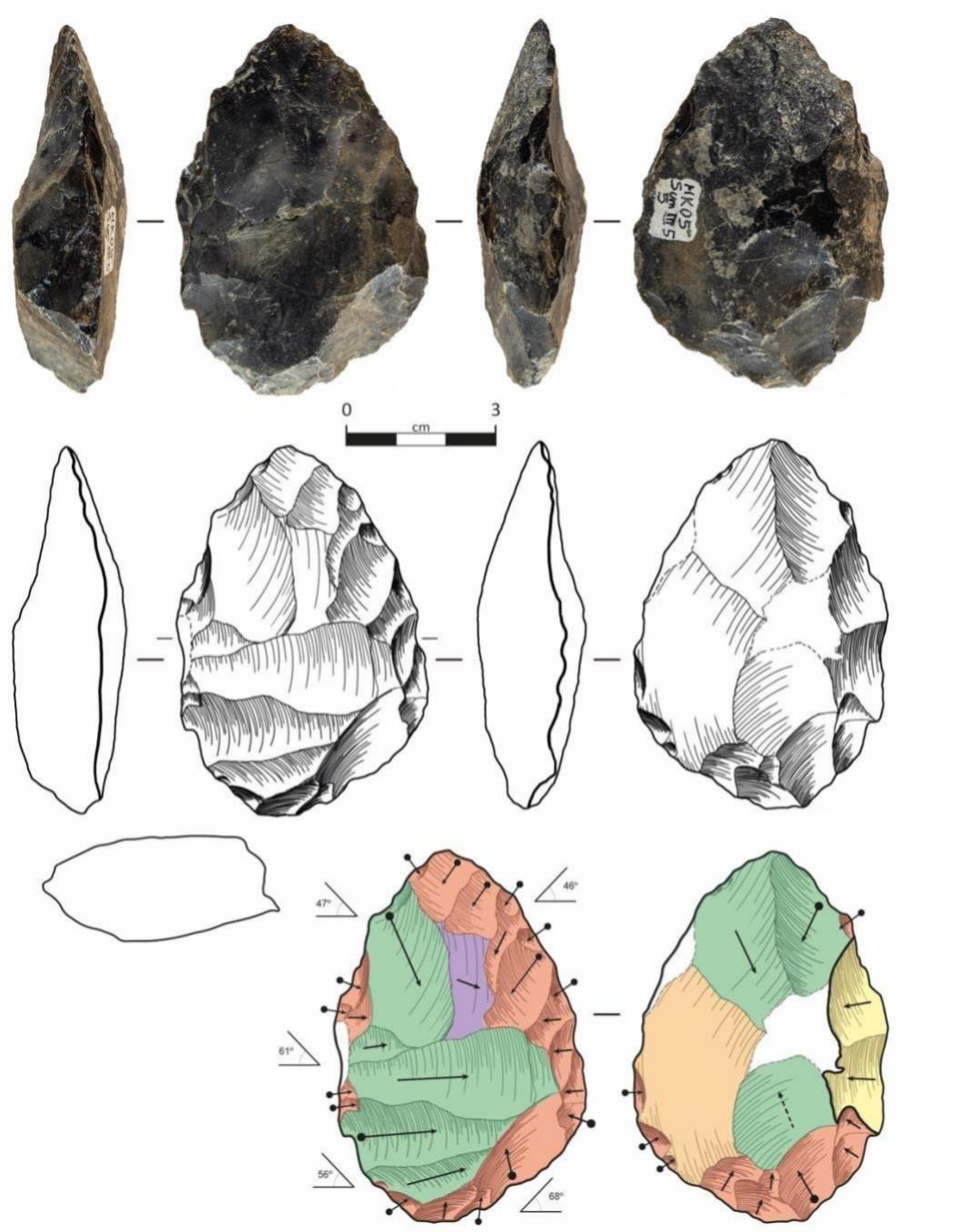

Supplementary Information Fig. C16. Level C: obsidian handaxe on an indeterminate flake with partial bifacial reduction.

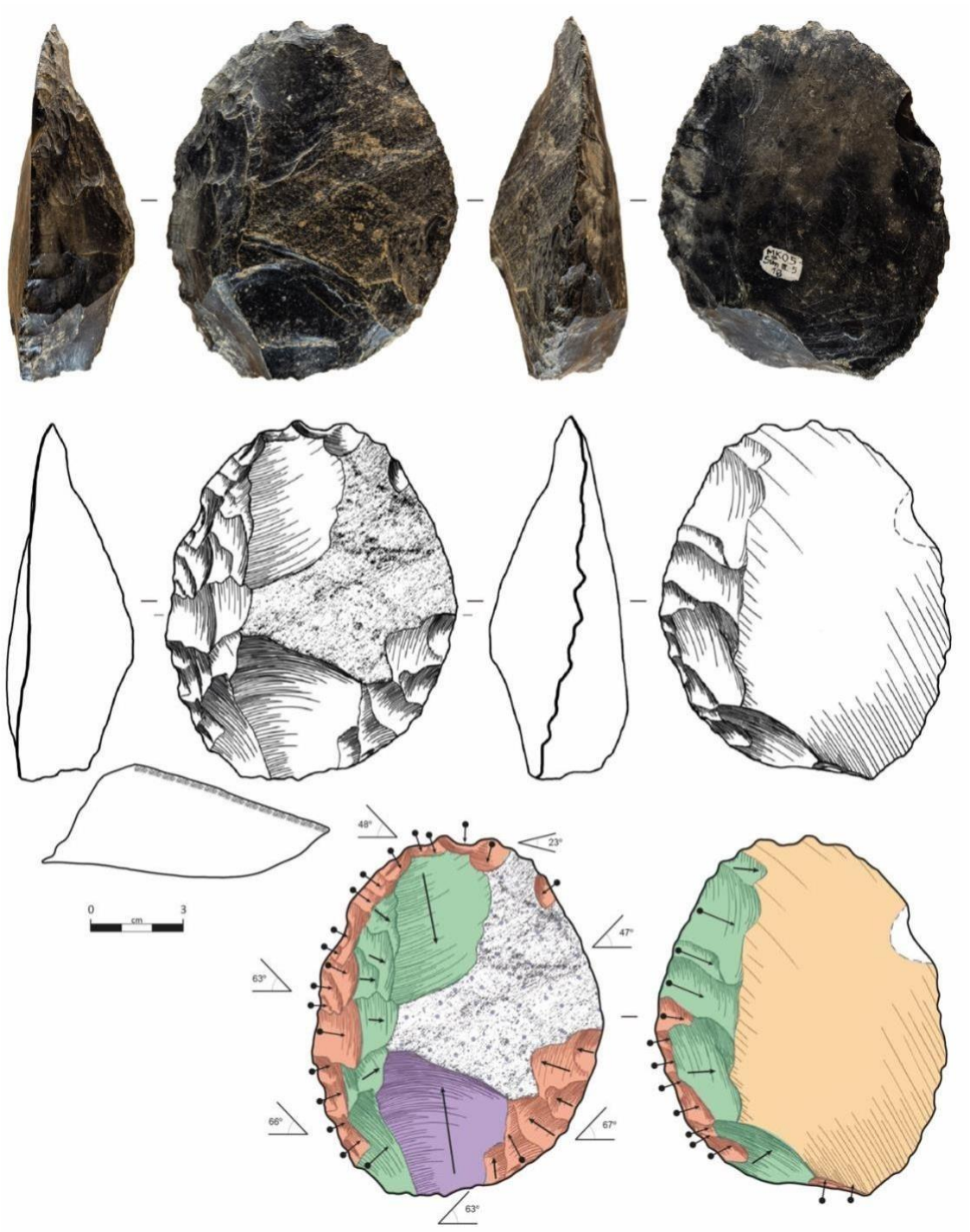

Supplementary Information Fig. C17. Level C: obsidian handaxe on a cortical flake with non-bifacial reduction.

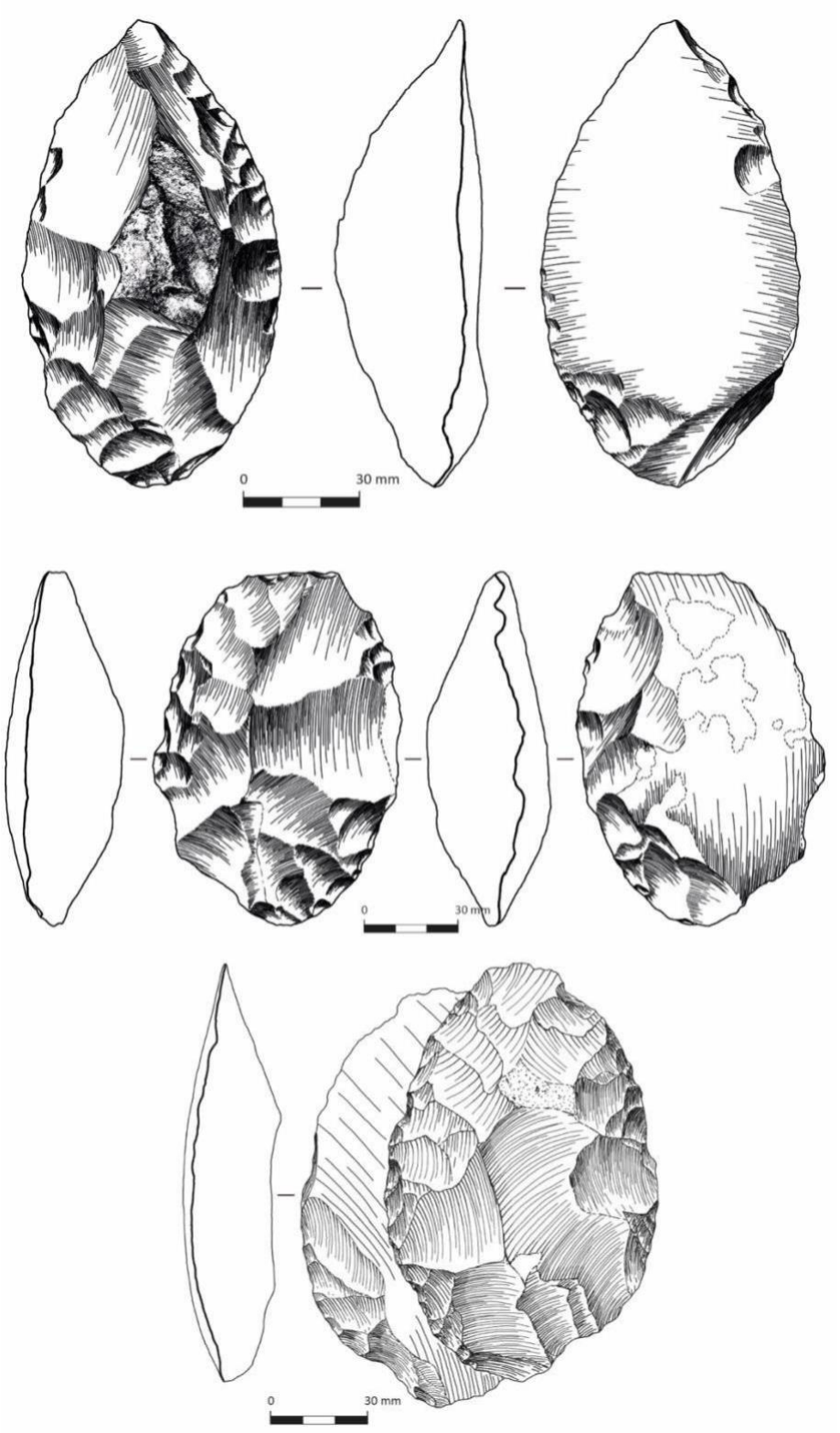

Supplementary Information Fig. C18. Level C: obsidian handaxes displaying various shaping degrees.

References

1 Oussedik, O. Site de Simburro III à Melka-Kunturé. *L'Ethiopie avant l'Histoire* **1**, 27-33 (1976).

2 Cressier, P. *Magnétostratigraphie du gisement pléistocène de Melka-Kunturé (Ethiopie). Datation des niveaux oldowayens et acheuléens*, Université Louis Pasteur, (1980).

3 Le Bourdonnec, F.-X. *Aspects archéométriques de la circulation de l'obsidienne préhistorique: développements analytiques et applications en Corse, Sardaigne et Ethiopie*, Université Michel de Montaigne Bordeaux 3, (2007).

4 Morgan, L. E. *et al.* A chronological framework for a long and persistent archaeological record: Melka Kunture, Ethiopia. *Journal of Human Evolution* **62**, 104-115, doi:10.1016/j.jhevol.2011.10.007 (2012).

5 Chavaillon, J. & Berthelet, A. in *Studies on the Early Paleolithic site of Melka Kunture, Ethiopia* (eds J. Chavaillon & M. Piperno), The archaeological sites of Melka Kunture, 25-80 (Istituto Italiano di Preistoria e Protostoria, 2004).

6 Geraads, D., Eisenmann, V. & Petter, G. in *Studies on the Early Paleolithic site of Melka Kunture, Ethiopia* (eds J. Chavaillon & M. Piperno), The large mammal fauna of the Oldowan sites of Melka Kunture, 169-192 (Istituto Italiano di Preistoria e Protostoria, 2004).

7 Perini, S., Muttoni, G., Monesi, E., Melis, R. T. & Mussi, M. Magnetochronology and age models of deposition of the Melka Kunture stratigraphic sequence (Upper Awash, Ethiopia) and age assessments of the main archeological levels therein contained. *Quaternary Science Reviews* **274**, 107259, doi:10.1016/j.quascirev.2021.107259 (2021).

8 Beaudet, A. *et al.* A new cercopithecoid dentognathic specimen attributed to Theropithecus from the late Early Pleistocene (c. 1 Ma) deposits of Simbiro, at Melka Kunture, Ethiopian highlands. *Comptes Rendus Palevol* **14**, 657-669, doi:https://doi.org/10.1016/j.crpv.2015.07.003 (2015).

9 An, X.-H. Morphological characteristics of phytoliths from representative conifers in China. *Palaeoworld* **25**, 116-127, doi:https://doi.org/10.1016/j.palwor.2016.01.002 (2016).

10 Ball, T. B. in *Plants, People and Places: Recent Studies in Phytolith Analysis* (eds M. Madella & D. Zurro), A survey of phytoliths produced by the vegetation of Dhofar, Oman, 29-40 (Oxbow books, 2007).

11 Barboni, D. & Bremond, L. Phytoliths of East African grasses: An assessment of their environmental and taxonomic significance based on floristic data. *Review of Palaeobotany and Palynology* **158**, 29-41, doi:https://doi.org/10.1016/j.revpalbo.2009.07.002 (2009).

12 Collura, L. V. & Neumann, K. Wood and bark phytoliths of West African woody plants. *Quaternary International* **434**, 142-159, doi:https://doi.org/10.1016/j.quaint.2015.12.070 (2017).

13 Garnier, A., Neumann, K., Eichhorn, B. & Lespez, L. Phytolith taphonomy in the middle- to late-Holocene fluvial sediments of Ounjougou (Mali, West Africa). *The Holocene* **23**, 416-431, doi:10.1177/0959683612463102 (2012).

14 Lisztes-Szabó, Z., Braun, M., Csík, A. & Pető, Á. Phytoliths of six woody species important in the Carpathians: characteristic phytoliths in Norway spruce needles. *Vegetation History and Archaeobotany* **28**, 649-662 (2019).

15 Mercader, J., Bennett, T., Esselmont, C., Simpson, S. & Walde, D. Phytoliths in woody plants from the Miombo woodlands of Mozambique. *Annals of Botany* **104**, 91-113 (2009).

16 Neumann, K., Fahmy, A. G., Müller-Scheeßel, N. & Schmidt, M. Taxonomic, ecological and palaeoecological significance of leaf phytoliths in West African grasses. *Quaternary International* **434**, 15-32, doi:https://doi.org/10.1016/j.quaint.2015.11.039 (2017).

17 Novello, A. *et al.* Phytolith signal of aquatic plants and soils in Chad, Central Africa. *Review of Palaeobotany and Palynology* **178**, 43-58, doi:https://doi.org/10.1016/j.revpalbo.2012.03.010 (2012).

18 Strömberg, C. A. E. *The origin and spread of grass-dominated ecosystems during the Tertiary of North America and how it relates to the evolution of hypsodonty in equids*, University of California, (2003).

19 Van de Vyver, T. *Fytolietenstudie van de Cyperaceae en Bolboschoenus maritimus in het bijzonder*, University of Ghent, (1999).

20 Kondo, R. & Sumida, D. The study of opal phytoliths of tree leaves. l. Opal phytoliths in gymnosperm and monocotyledonous angiosperm tree leaves. *Jpn. Sci. Soil Manure* **49**, 138-144 (1978).

21 Neumann, K. *et al.* International Code for Phytolith Nomenclature (ICPN) 2.0. *Annals of Botany* **124**, 189-199, doi:10.1093/aob/mcz064 (2019).

22 Barboni, D. (Dryad, 2021).

23 Arráiz, H. *et al.* Paleovegetation changes accompanying the evolution of a riverine system at the BK paleoanthropological site (Upper Bed II, Olduvai Gorge, Tanzania). *Palaeogeography, Palaeoclimatology, Palaeoecology* **488**, 84-92, doi:https://doi.org/10.1016/j.palaeo.2017.05.010 (2017).

24 Bamford, M., Albert, R. & Cabanes, D. Plio–Pleistocene macroplant fossil remains and phytoliths from Lowermost Bed II in the eastern palaeolake margin of Olduvai Gorge, Tanzania. *Quaternary International* **148**, 95-112, doi:10.1016/j.quaint.2005.11.027 (2006).

25 Douglas, M. S. & Smol, J. P. Periphytic diatom assemblages from high arctic ponds. *Journal of Phycology* **31**, 60-69 (1995).

26 Bremond, L., Boom, A. & Favier, C. Neotropical C3/C4 grass distributions–present, past and future. *Global Change Biology* **18**, 2324-2334 (2012).

27 Bremond, L. *et al.* Phytolith indices as proxies of grass subfamilies on East African tropical mountains. *Global and Planetary Change* **61**, 209-224, doi:https://doi.org/10.1016/j.gloplacha.2007.08.016 (2008).

28 Bocherens, H. in *Biogeochemical Approaches to Paleodietary Analyses* (eds M.A. Katzenberg & S.H. Ambrose), Preservation of isotopic signals (13C,15N) in Pleistocene mammals, 65-88 (Kluwer Academic/Plenum Publishers, 2000).

29 Cerling, T. E. & Harris, J. M. Carbon isotope fractionation between diet and bioapatite in ungulate mammals and implications for ecological and paleo-ecological studies. *Oecologia* **120** (1999).

30 Cerling, T. E. *et al.* Stable isotope ecology of the common hippopotamus. *Journal of Zoology* **276**, 204–212 (2008).

31 Clementz, M. T. & Koch, P. L. Differentiating aquatic mammal habitat and foraging ecology with stable isotopes in tooth enamel. *Oecologia* **129**, 461-472 (2001).

32 Clementz, M. T., Holroyd, P. A. & Koch, P. L. Identifying aquatic habits of herbivorous mammals through stable isotope analysis. *Palaios* **23**, 574-585 (2008).

33 Calvin, M. & Benson, A. A. The path of carbon in photosynthesis. *Science* **107**, 476-480 (1948).

34 Ehleringer, J. R. & Monson, R. K. Evolutionary and ecological aspects of photosynthetic pathway variation. *Annual Review of Ecology and Systematics*, 411-439 (1993).

35 Kohn, M. J. & Cerling, T. E. in *Reviews in Mineralogy and Geochemistry 48* (eds M.J. Kohn, J. Rakovan, & J.M. Hughes), Stable isotope compositions of biological apatite, 455-488 (Mineralogical Society of America, 2002).

36 Bocherens, H., Koch, P. L., Mariotti, A., Geraads, D. & Jaeger, J.-J. Isotopic biogeochemistry (^{13}C, ^{18}O) of mammal enamel from African Pleistocene hominid sites: implications for the preservation of paleoclimatic isotopic signals. *PALAIOS* **11**, 306-318, doi:10.2307/3515241 (1996).

37 Bocherens, H. & Drucker, D. Terrestrial Teeth and Bones. *Encyclopedia of Quaternary Science* **1**, 304-314 (2013).

38 Kohn, M. J. Predicting animal δ18O: accounting for diet and physiological adaptation. *Geochim. Cosmochim. Acta* **60**, 4811-4829 (1996).

39 Levin, N. E., Simpson, S. W., Quade, J., Cerling, T. E. & Frost, S. R. in *The geology of early humans in the Horn of Africa* Vol. 446 (eds J. Quade & J.G. Wynn), Herbivore enamel carbon isotopic composition and the environmental context of Ardipithecus at Gona, Ethiopia, 215-234 (Geological Society of America Special Paper, 2008).

40 Levin, N. E., Cerling, T. E., Passey, B. H., Harris, J. M. & Ehleringer, J. R. A stable isotope aridity index for terrestrial environments. *Proceedings of the National Academy of Sciences* **103**, 11201-11205 (2006).

41 Harris, J., Cerling, T., Leakey, M. & Passey, B. Stable isotope ecology of fossil hippopotamids from the Lake Turkana Basin of East Africa. *Journal of Zoology* **275**, 323-331 (2008).

42 Souron, A., Balasse, M. & Boisserie, J.-R. Intra-tooth isotopic profiles of canines from extant Hippopotamus amphibius and late Pliocene hippopotamids (Shungura Formation, Ethiopia): Insights into the seasonality of diet and climate. *Palaeogeography, Palaeoclimatology, Palaeoecology* **342-343**, 97-110, doi:10.1016/j.palaeo.2012.05.007 (2012).

43 Bocherens, H., Fizet, M. & Mariotti, A. Diet, physiology and ecology of fossil mammals as inferred from stable carbon and nitrogen isotope biogeochemistry: implications for

Pleistocene bears. *Palaeogeography, Palaeoclimatology, Palaeoecology* **107**, 213-225 (1994).

44 Wright, L. E. & Schwarcz, H. P. Correspondence between stable carbon, oxygen and nitrogen isotopes in human tooth enamel and dentine: infant diets at Kaminaljuyú. *Journal of Archaeological Science* **26**, 1159-1170 (1999).

45 Koch, P. L., Tuross, N. & Fogel, M. L. The Effects of Sample Treatment and Diagenesis on the Isotopic Integrity of Carbonate in Biogenic Hydroxylapatite. *Journal of Archaeological Science* **24**, 417-429, doi:10.1006/jasc.1996.0126 (1997).

46 Feibel, C. S., Brown, F. H. & McDougall, I. Stratigraphic context of fossil hominids from the Omo Group deposits: northern Turkana Basin, Kenya and Ethiopia. *American Journal of Physical Anthropology* **78**, 595-622 (1989).

47 Heinzelin, J. *The Omo Group. Archives of the International Omo Research Expedition*. (Musée Royal de l'Afrique Centrale, 1983).

48 McDougall, I. & Brown, F. H. Geochronology of the pre-KBS tuff sequence, Omo Group, Turkana Basin. *Journal of the Geological Society* **165**, 549-562 (2008).

49 Boisserie, J.-R. *et al.* Diets of modern and late Miocene hippopotamids: Evidence from carbon isotope composition and micro-wear of tooth enamel. *Palaeogeography, Palaeoclimatology, Palaeoecology* **221**, 153-174, doi:https://doi.org/10.1016/j.palaeo.2005.02.010 (2005).